Neurobiology of Disease 186 (2023) 106274

Contents lists available at ScienceDirect

Neurobiology of Disease

journal homepage: www.elsevier.com/locate/ynbdi

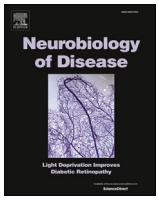

Distinct impacts of alpha-synuclein overexpression on the hippocampal epigenome of mice in standard and enriched environments

Samantha L. Schaffner [a,b], Zinah Wassouf [c,1], Thomas Hentrich [c,2], Melanie Nuesch-Germano [d], Michael S. Kobor [a,b], Julia M. Schulze-Hentrich [c,*,2]

[a] Edwin S. H. Leong Centre for Healthy Aging, Faculty of Medicine, 117-2194 Health Sciences Mall, University of British Columbia, V6T 1Z3 Vancouver, BC, Canada
[b] Department of Medical Genetics, Centre for Molecular Medicine and Therapeutics, British Columbia Children's Hospital Research Institute, University of British Columbia, V5Z 4H4 Vancouver, BC, Canada
[c] Institute of Medical Genetics and Applied Genomics, University of Tübingen, 72076 Tübingen, Germany
[d] University of Bonn, 53115 Bonn, Germany

ARTICLE INFO

Keywords:
Alpha-synuclein
Epigenetics
Multiomics integration
Gene-environment interaction

ABSTRACT

Elevated alpha-synuclein (*SNCA*) gene expression is associated with transcriptional deregulation and increased risk of Parkinson's disease, which may be partially ameliorated by environmental enrichment. At the molecular level, there is emerging evidence that excess alpha-synuclein protein (aSyn) impacts the epigenome through direct and/or indirect mechanisms. However, the extents to which the effects of both aSyn and the environment converge at the epigenome and whether epigenetic alterations underpin the preventive effects of environmental factors on transcription remain to be elucidated. Here, we profiled five DNA and histone modifications in the hippocampus of wild-type and transgenic mice overexpressing human *SNCA*. Mice of each genotype were housed under either standard conditions or in an enriched environment (EE) for 12 months. *SNCA* overexpression induced hippocampal CpG hydroxymethylation and histone H3K27 acetylation changes that associated with genotype more than environment. Excess aSyn was also associated with genotype- and environment-dependent changes in non-CpG (CpH) DNA methylation and H3K4 methylation. These H3K4 methylation changes included loci where the EE ameliorated the impacts of the transgene as well as loci resistant to the effects of environmental enrichment in transgenic mice. In addition, select H3K4 monomethylation alterations were associated with changes in mRNA expression. Our results suggested an environment-dependent impact of excess aSyn on some functionally relevant parts of the epigenome, and will ultimately enhance our understanding of the molecular etiology of Parkinson's disease and other synucleinopathies.

1. Introduction

The *SNCA* gene encodes alpha-synuclein (aSyn), a multifunctional protein important for neuronal differentiation, synaptic transmission, and dopamine synthesis (Villar-Piqué et al., 2016). Individuals carrying *SNCA* gene multiplications, point mutations impairing aSyn function and/or enhancing its fibrillization (such as A53T, E46K, and A30P), or promoter alleles increasing expression of aSyn are at increased risk of

Abbreviations: aSyn, alpha-synuclein protein; BAC, bacterial artificial chromosome; BS, bisulfite; CpG, cytosine-phosphate-guanine dinucleotide; DEG, differentially expressed gene; DNAm, DNA methylation; DNAhm, DNA hydroxymethylation; DPBS, Dulbecco's phosphate-buffered saline; EDTA, ethylenediaminetetraacetic acid; EE, enriched environment; FC, fold change; GO, Gene Ontology; IQR, interquartile range; MAPQ, mapping quality score; oxBS, oxidative bisulfite; ox-RRBS, oxidative reduced-representation bisulfite sequencing; PD, Parkinson's disease; PTM, posttranslational modification; RRBS, reduced-representation bisulfite sequencing; SDS, sodium dodecyl sulfate; SE, standard environment; TG, transgenic; TG_{EE}, alpha-synuclein transgenic mice housed in an enriched environment; TG_{SE}, alpha-synuclein transgenic mice housed in the standard environment; TSS, transcription start site; WT, wild-type; WT_{EE}, wild-type mice housed in an enriched environment; WT_{SE}, wild-type mice housed in the standard environment.

* Corresponding author at: Saarland University, Genetics/Epigenetics, Campus, Building A2.4, 66123 Saarbrücken, Germany.
E-mail addresses: sschaffner@bcchr.ca (S.L. Schaffner), zw4@sanger.ac.uk (Z. Wassouf), mnueschg@uni-bonn.de (M. Nuesch-Germano), michael.kobor@ubc.ca (M.S. Kobor), julia.schulze-hentrich@uni-saarland.de (J.M. Schulze-Hentrich).
[1] Present address: Wellcome Sanger Institute, Wellcome Genome Campus, Hinxton, Cambridgeshire, UK.
[2] Present address: Department of Genetics/Epigenetics, Faculty NT, Saarland University, 66041 Saarbrücken, Germany.

https://doi.org/10.1016/j.nbd.2023.106274
Received 2 May 2023; Received in revised form 18 August 2023; Accepted 27 August 2023
Available online 28 August 2023

developing Parkinson's disease (PD) and other synucleinopathies due to excess production, loss of function, and/or misfolding of aSyn protein. This excess aSyn contributes to the formation of Lewy body aggregates in the brain, a hallmark of PD associated with neuronal toxicity (Villar-Piqué et al., 2016; Chiba-Falek and Nussbaum, 2001; Maraganore et al., 2006; Chartier-Harlin et al., 2004). aSyn pathology can affect multiple brain regions in PD, most notably the substantia nigra; however, its accumulation in the hippocampus has been implicated in early non-motor symptoms of PD, such as dementia, impulse control disorder, and fatigue (Calabresi et al., 2013). As aSyn buildup and neuronal loss in PD occur gradually over several decades, there is increasing interest in lifestyle intervention strategies to prevent or slow the course of disease onset in individuals with known or unknown genetic risk factors (Chen and Ritz, 2018). The responsiveness of the hippocampus to increased sensory information from new and changing environments, combined with its role in early nonmotor manifestations of synucleinopathies, makes this brain region an attractive target for such interventions (Kempermann et al., 1997).

Physical activity and cognitive stimulation, training, and rehabilitation are two well-studied actionable strategies that have been shown to reduce the risk of developing PD and slow symptom progression in humans (Vemuri et al., 2016; Ascherio and Schwarzschild, 2016; Crotty and Schwarzschild, 2020). In animal models without genetic modifications, an enriched environment (EE) paradigm with increased physical, social, and cognitive stimulation can be used to mimic the neuroprotective effects of exercise, and has shown promise in combating aging, neurodegenerative, and neuroinflammatory phenotypes (Nithianantharajah and Hannan, 2006; Wassouf and Schulze-Hentrich, 2019). EE setups typically consist of larger cages housing more animals, with the provision of frequently rearranged objects, toys, and exercise wheels. There is accumulating evidence that EE shows protective effects on the hippocampus, including induction of neurogenesis and upregulated expression of genes involved in learning and memory in wild-type (WT) mice, as well as downregulated expression of aSyn and buffering of transcriptional changes induced by *SNCA* overexpression in transgenic (TG) mice (Crotty and Schwarzschild, 2020; Wassouf and Schulze-Hentrich, 2019; Wassouf et al., 2018; Irier et al., 2014; Zhang et al., 2018; Zocher et al., 2021). At the same time, EE has also been shown to prevent age-associated epigenetic drift at the level of DNA methylation (DNAm), and to alter genome-wide hippocampal DNA hydroxymethylation (DNAhm) patterns (Irier et al., 2014; Zocher et al., 2021). In the mouse cortex, EE alters DNAm, promoter and gene body histone posttranslational modifications (PTMs), and gene expression, and increases enhancer and promoter chromatin accessibility (Espeso-Gil et al., 2021). However, the mechanisms by which EE impacts gene regulation and epigenetics in the context of genetic risk of PD are only beginning to be explored.

Here, we assessed the impacts of *SNCA* overexpression on DNAm, DNAhm, and three enhancer- and promoter-associated histone PTMs—H3K4 monomethylation (H3K4me1), H3K4 trimethylation (H3K4me3), and H3K27 acetylation (H3K27ac)—in mice housed under a standard environment (SE) paradigm or EE to examine epigenetic alterations at transcriptional regulatory elements. These observations were integrated with previously generated RNA-seq data from the hippocampus of the same mice profiled for DNAm and DNAhm in the present study (Wassouf et al., 2018). The results showed that the impacts of *SNCA* overexpression on DNAhm and H3K27ac were consistent between environments, while *SNCA* overexpression impacted H3K4 methylation and DNAm in an environment-dependent manner. The EE partially restored H3K4me1 levels in TG mice, suggesting a potential role of H3K4me1 in the EE-induced adaptive response to excess hippocampal aSyn level.

2. Materials and methods

2.1. Generation of aSyn-expressing mice

Generation of aSyn-expressing mice was described previously (Wassouf et al., 2018). Briefly, a bacterial artificial chromosome (BAC) construct containing the entire human *SNCA* gene locus and its flanking regions was used to generate a TG mouse model in C57BL/6 N mice obtained from Charles River (Yamakado et al., 2012; Nuber et al., 2013). Homozygosity was confirmed by quantitative real-time PCR (Light-Cycler 480; Roche, Basel, Switzerland) after weaning and was confirmed at sacrifice.

2.2. Study design and environmental enrichment

The study design was described previously (Wassouf et al., 2018). Briefly, WT and TG animals were assigned randomly to either SE (3–4 mice/cage, Type II long) or EE (8 mice/cage, larger cages with additional bedding and nesting material, Type IV) after weaning; only females were used in the experiments to avoid aggression between males with long-term housing in EE (Nithianantharajah and Hannan, 2006; Marashi et al., 2003; Hüttenrauch et al., 2016). Enriched cages were supplied with a variety of objects as well as tunnels, climbing cubes, saucer wheels, and running wheels, which were rearranged three times a week over a period of 12 months.

2.3. RNA and DNA extraction

Total RNA and DNA were extracted simultaneously using an AllPrep DNA/RNA Mini Kit (Qiagen, Hilden, Germany) according to the manufacturer's protocol. Quality was assessed with an Agilent 2100 Bioanalyzer (Agilent Technologies, Santa Clara, CA, USA).

2.4. RNA sequencing and differential expression analysis

RNA-seq and bioinformatics analyses were performed as described previously, and the data are publicly available through Gene Expression Omnibus (GSE96961) (Wassouf et al., 2018). Briefly, hippocampal RNA was prepared using a TruSeq RNA Sample Prep Kit (Illumina, San Diego, CA, USA) and 500 ng of total RNA for each sequencing library. Poly(A)-selected single-end sequencing libraries (read lengths of 50 and 65 bp) were generated according to the manufacturer's instructions. All libraries were sequenced on an Illumina HiSeq 2500 platform at a depth of 10–20 million reads each. RNA-seq read quality was assessed with FastQC v0.11.4, and reads were aligned to a custom-built genome composed of the Ensembl *Mus musculus* genome v82 and the human *SNCA* transgene using STAR v2.4.2a (Babraham, 2010; Dobin et al., 2013). DESeq2 was used to normalize read counts, and 12,287 genes with ≥ 50 reads covered were assessed for differential expression using the generalized linear model $t \sim g + e + g \times e$, where t represents gene expression, g represents genotype, and e represents environment (Love et al., 2014). Genes were considered differentially expressed at $|\log2FC| \geq 0.3$ and $p_{adj} \leq 0.05$.

2.5. Reduced-representation bisulfite sequencing and differential DNA (hydroxy)methylation analysis

Reduced-representation bisulfite sequencing (RRBS) library preparation was performed as described previously; the methods outlined below are reproduced with permission from (Schaffner et al., 2022). RRBS libraries were prepared following the protocol reported previously (Gu et al., 2011) using 400 ng of genomic DNA per sample. An aliquot of 0.4 ng of unmethylated phage lambda DNA per sample was added during the *Msp*I digestion step as a control for bisulfite conversion efficiency, and *Msp*I reactions were performed with incubation at 37 °C for 16 h. Digested DNA was end-repaired, and then purified using AMPure

XP magnetic beads (Beckman Coulter Life Sciences, Brea, CA, USA) at 2× concentration, and 0.1 μM methylated adapters (Integrated DNA Technologies, Coralville, IA, USA) were used in ligation reactions. Ligated DNA was purified with 1.5× magnetic beads and quantified using a Qubit dsDNA HS Assay Kit (Thermo Fisher Scientific, Waltham, MA, USA). Eight samples per lane were pooled in equimolar amounts, and each pool was split into two aliquots for oxidative bisulfite (oxBS) and bisulfite (BS) conversion using the NuGEN TrueMethyl oxBS Module (NuGEN Technologies, San Carlos, CA, USA). One aliquot was subjected to oxidation, while the second aliquot was subjected to mock oxidation and the BS conversion protocol was then applied to both. Libraries were then amplified by PCR with Pfu Turbo Cx HotStart DNA polymerase for 14 cycles (Agilent Technologies). Size selection (200–550 bp) was performed using a 0.55× AMPure beads wash (Agilent Technologies) followed by two 1.2× washes for cleanup. The final libraries were eluted in 25 μL of Qiagen EB Buffer (Qiagen), and quality was assessed by PCR, spectrophotometry, fluorometry, and using a DNA high-sensitivity chip (Agilent Technologies). Then, 75 bp paired-end sequencing was conducted with Illumina HiSeq 2500 by the Michael Smith Genome Sciences Centre (Vancouver, BC, Canada). Raw RRBS data are publicly available through Gene Expression Omnibus (GSE228961).

BSMAP was used to align reads to the mm10 and phage lambda genomes (*Msp*I-digested RRBS mode, 5 mismatches permitted, no gaps, 20–500 bp fragment size, reporting only uniquely mapped reads) and to calculate methylation ratios (Xi and Li, 2009). Sequence data were assessed for quality before and after alignment using FastQC software (Babraham, 2010). Following alignment, reads were sorted and filtered for mapping quality (MAPQ) score > 10 using SAMtools (Li et al., 2009). Methylation ratio data for cytosine sites covered in all samples were then analyzed using R ver. 3.6.3. Bisulfite conversion efficiency was confirmed by assessing mean methylation levels across all cytosines in lambda-aligned samples, which was < 1% in all 16 instances. Outliers were assessed separately in oxBS and BS data using principal component analysis, with median read coverage < 20× across all cytosines, sample-sample correlation < 0.8, β distributions, *detectOutlier* from the `lumi` R package, and *outlyx* from the `wateRmelon` R package (Du et al., 2008; Pidsley et al., 2013). Samples that failed three or more outlier checks in the oxBS or the oxBS and BS data sets (one replicate each of WT_{SE}, TG_{SE}, and TG_{EE}) were removed from both prior to DNAhm estimation and differential (hydroxy)methylation analysis.

For the remaining 13 samples, cytosines were filtered with a minimum read depth of 10× and a maximum read depth of the 99.9%-quantile of coverage. The oxBS β values were used to represent DNAm, while BS − oxBS values were used to represent DNAhm, with the 95%-quantile of negative hmC values generated after subtraction used as the detectability threshold (Lunnon et al., 2016). We removed cytosines with ≤ 10% variability between groups (calculated using the 10th to 90th interquartile reference range for each cytosine) to reduce the multiple testing burden for differential DNA(*h*)m analysis, and excluded cytosines on the X chromosome.

Differential DNA(*h*)m analysis was conducted separately for cytosine-phosphate-guanine dinucleotide (CpG) and non-CpG (CpH) sites with linear regression, using the model $\mathrm{DNA}(h)\mathrm{m} \sim g + e + g \times e$, where *g* represents genotype and *e* represents environment. Model bias and inflation were calculated in each data set using the `bacon` R package, and were assessed visually using *p*-value histograms and quantile-quantile (Q-Q) plots (Table A.1, Fig. A.1, A.2) (van Iterson et al., 2017). For differential DNAhm analysis, group labels were also shuffled to ensure lack of inflation under a null model (Fig. A.2). The *p*-values were adjusted for multiple comparisons using the Benjamini–Hochberg method. Cytosines were considered differentially methylated at $p_{adj} \leq 0.05$ and $|\Delta\beta| \geq 0.1$, chosen to represent the minimum detectable difference in DNA(*h*)m according to the 10× read coverage filter. The *skewness.norm.test* function from the `normtest` R package was used to assess Δβ skewness, with 1000 Monte Carlo simulations (https://cran.r-project.org/web/packages/normtest/normtest.pdf).

2.6. Chromatin immunoprecipitation sequencing and differential binding analysis

Hippocampal tissue from an additional set of mice housed under the same experimental paradigm ($n = 4$ each WT_{SE}, TG_{SE}, WT_{EE}, and TG_{EE}) was homogenized with a glass homogenizer in Dulbecco's phosphate-buffered saline (DPBS) + 0.1% NP-40 and protease inhibitors (ethylenediaminetetraacetic acid [EDTA]-free) on ice. We cross-linked chromatin and DNA by adding formaldehyde (methanol-free; Thermo Fisher Scientific) to a final concentration of 1% and incubation on a rotating wheel at 25 °C for 10 min. Glycine was added to quench the cross-linking reaction at a final concentration of 0.125 M at 25 °C. After 5-min incubation with glycine, the reaction mixture was centrifuged at 10,000 ×*g* for 30 s at 4 °C and washed twice with 1 mL of cold DPBS. The pellet was resuspended in radioimmunoprecipitation assay (RIPA) sodium dodecyl sulfate (SDS) buffer (140 mM NaCl, 1 mM EDTA, pH 8.0, 1% Triton X-100, 0.1% sodium deoxycholate, 10 mM Tris-Cl, pH 8.0, 1% SDS) supplemented with Roche Complete Protease Inhibitor Cocktail (Roche), incubated at 4 °C for 10 min, and then sheared by ultrasonication (Covaris, Boston, MA, USA). An aliquot was taken to check DNA size on an Agilent 2100 Bioanalyzer (Agilent Technologies) and immunoprecipitation was performed when DNA was sheared to fragments of 150–300 bp. The sample was then diluted 10× in IP no SDS buffer (150 mM NaCl, 1% NP-40, 0.5% sodium deoxycholate, 50 mM Tris-HCl, pH 8.0, 2 mM EDTA) supplemented with Roche Complete Protease Inhibitor Cocktail (Roche), pre-cleared with protein A magnetic beads (Dynabeads; Invitrogen, Waltham, MA, USA) for 1 h at 4 °C, and subjected to immunoprecipitation with histone modification-specific ChIP-grade antibody. The sample was incubated overnight at 4 °C, and then protein A magnetic beads were added followed by incubation for 2 h at 4 °C. Beads were washed twice with cold IP buffer with 0.1% SDS and protease inhibitors, three times with wash buffer (100 mM Tris-HCl, pH 8.0, 500 mM LiCl, 1% *v*/v NP-40, 1% *w/v* sodium deoxycholate, 2 mM EDTA), and twice with Tris-EDTA buffer. After the last wash, the supernatant was removed and beads were resuspended in 1 mM Tris (pH 8.0) and RNase A (0.1 μg/μL), followed by incubation for 30 min at 37 °C. Reverse cross-linking was performed overnight at 65 °C in 100 mM Tris-HCl (pH 8.0), 20 mM EDTA, 2% SDS, and proteinase K (0.5 μg/μL). DNA was purified with SureClean (Meridian Bioscience, Cincinnati, OH, USA) and DNA concentration was measured with a Qubit dsDNA HS Assay Kit (Thermo Fisher Scientific). Aliquots of 3 ng of ChIPed DNA were used for library generation using a NEBNext Ultra II DNA Library Prep Kit for Illumina (New England Biolabs, Ipswich, MA, USA), size was determined with an Agilent High Sensitivity DNA Kit on an Agilent Bioanalyzer (Agilent Technologies), and sequencing was performed on an Illumina NovaSeq 6000 instrument (Illumina) according to the manufacturer's instructions.

The read quality of ChIP-seq data was assessed using FastQC, and reads were aligned to the mouse genome (mm10) using Bowtie2 (Babraham, 2010; Langmead and Salzberg, 2012). Aligned reads were filtered and only reads with MAPQ score ≥ 30 were retained. PCR duplicates were marked using SAMtools and peak calling using MACS2 (v2.1.2) was performed using the default settings with a q-value cutoff of 0.05 and with the input (10% of the sample before immunoprecipitation) as the control (https://github.com/taoliu/MACS) (Li et al., 2009). Broad peaks were called for H3K27ac and H3K4me1 data, while narrow peaks were called for H3K4me3 data. The resulting peaks were filtered and ENCODE blacklist regions were removed using bedtools (https://bedtools.readthedocs.io/en/latest/). Differential binding analysis was performed using `DiffBind` on consensus ChIP-seq peaks present in at least two replicates of the same experimental group (Stark and Brown, 2011). `ChIPseeker` was used to annotate ChIP-seq peaks (Yu et al., 2015).

2.7. Hierarchical clustering analysis

Unsupervised hierarchical clustering with multiscale bootstrap resampling was performed separately for each of the data sets analyzed in this study using the *pvclust()* function from the `pvclust` package in R ver. 3.6.3, with clusters considered stable at approximately unbiased (AU) $p < 0.05$ (Suzuki and Shimodaira, 2006). Input to the *pvclust()* function consisted of DNAm β values for 329,507 CpGs or 75,533 CpHs used for differential methylation analysis, DNAhm β values for 19,308 CpGs or 170 s CpHs used for differential DNAhm analysis, and 120,387 H3K4me1 peaks, 36,517 H3K4me3 peaks, and 97,234 H3K27ac peaks each used in respective differential binding analyses. Clustering patterns generated from *pvclust()* were visualized using the *heatmap.2()* function from the `gplots` package in R ver. 3.6.3 (Warnes et al., 2022). For CpG methylation, CpH methylation, H3K4me1, and H3K27ac data sets, the top most variable 20,000 cytosines or peaks (calculated using interquartile reference range) were used as input for *heatmap.2()* to aid visualization and to not exceed memory limitations. All 19,308 CpGs and 36,517 peaks were used as input for CpG hydroxymethylation and H3K4me3, respectively.

2.8. Gene feature annotation

DNAm, and DNAhm data were annotated to gene features using `annotatr` with the mm10 genome, and ChIP-seq data were annotated using `ChIPseeker` (Yu et al., 2015; Cavalcante and Sartor, 2017). We selected one gene feature and one CpG island feature per cytosine according to the longest transcript mapping to each position. Active and poised enhancers and active promoters were defined using the H3K4me1, H3K27ac, and H3K4me3 ChIP-seq data generated in this study, based on the established approach (Creyghton et al., 2010). Consensus peaks common to all groups were used. Enhancers were defined by filtering out H3K4me1 peaks ± 2 kb from transcription start site (TSS) regions, and were considered "active" if an H3K27ac peak was within a distance of ± 4 kb, otherwise they were considered "poised." Active promoters were defined as H3K27ac peaks intersecting the TSS within a ± 2-kb window.

2.9. Gene ontology enrichment

Gene Ontology (GO) enrichment analysis was performed with `gProfiler2` by overrepresentation analysis with a hypergeometric test for significance (Kolberg et al., 2020). The *p*-values were adjusted with the "*fdr*" method in the *gost()* function. Genes significant in each analysis (mapping to cytosines passing $|\Delta\beta| \geq 0.1$ and $p_{adj} \leq 0.05$ in the RRBS data sets, or to peaks passing $|\log2FC| \geq 0.5$ and $p_{adj} \leq 0.05$ in the ChIP-seq data sets) were used as input, and were compared to a custom background of all genes covered in the final RRBS or ChIP-seq data sets.

2.10. Mouse hippocampal cell type enrichment

To examine whether changes in the hippocampal epigenome of the mice assessed in this study could be attributed to particular cell types, we performed enrichment analysis of differentially hydroxymethylated CpGs and differentially bound H3K27ac, H3K4me1, and H3K4me3 peaks for genes expressed in five hippocampal cell types, based on mouse single-cell RNA-seq data reported previously (Zeisel et al., 2015). For this purpose, we subset the reference single-cell data to genes covered in the data set in question (i.e., CpG hydroxymethylation, H3K27ac, H3K4me1, or H3K4me3), and calculated the overlap of genes passing significance and effect size cutoffs in each analysis with genes attributed to each hippocampal cell type. The two-sided Fisher's exact test was used to calculate whether the number of differentially regulated genes attributed to each cell type was higher or lower than expected by chance, with a significance cutoff of $p < 0.05$.

3. Results

3.1. CpG hydroxymethylation and histone posttranslational modification data separated by SNCA genotype in unsupervised hierarchical clustering analysis

To study the impacts of *SNCA* overexpression in the brain, we used a TG mouse model carrying a BAC containing the full-length human *SNCA* gene and its native human regulatory elements, with approximately 6-fold overexpression of *SNCA* mRNA described previously (Wassouf et al., 2018; Yamakado et al., 2012; Nuber et al., 2013). The human *SNCA* transgene and endogenous murine aSyn protein were expressed primarily in the forebrain, including the olfactory bulb, cortex, striatum, and hippocampus (Wassouf et al., 2018). WT or *SNCA* TG mice were raised from weaning to the age of 12 months in either the SE or EE (WT_{SE}, WT_{EE}, TG_{SE}, and TG_{EE}, respectively; $n = 4$ biological replicates per group), followed by sacrifice and extraction of hippocampal RNA and DNA (Fig. 1A). In this study, DNAm was assessed by oxidative RRBS (ox-RRBS) at 329,507 CpGs and 75,533 CpHs (where H represents A, T, or C), which were covered in all animals at depth ≥ 10 reads and ≤ 99.9%-quantile of coverage, and which had variable levels of DNAm across all animals (≥ 10% of interquartile range (IQR) between the 10th and 90th percentile of CpG methylation; GSE228961). DNAhm was assessed by paired BS and oxBS conversion of RRBS libraries, with 19,308 CpGs and 170 CpHs remaining after filtering both the BS and oxBS libraries according to the above coverage and variability metrics, and subsetting to CpGs with $|\beta|$ values exceeding the 95%-quantile of negative DNAhm measurements obtained after subtraction of the oxBS from BS signal (Lunnon et al., 2016) (GSE228961). After outlier removal from the ox-RRBS data, 3–4 mice per group remained (biological replicates; WT_{SE}, $n = 4$; WT_{EE}, $n = 3$; TG_{SE}, $n = 3$; TG_{EE}, $n = 3$). Gene expression for these mice was reported previously (12,286 genes passing quality control [QC]) (Wassouf et al., 2018) (GSE96961). We also profiled a second set of mice of the same genotypes raised under the same environmental conditions for histone PTMs to gain further insight into chromatin regulation ($n = 4$ biological replicates per group) (Fig. 1A). The genomic localizations of H3K4me1 (associated with active and poised enhancers), H3K4me3 (associated with promoters), and H3K27ac (associated with active enhancers and promoters) were assessed by chromatin immunoprecipitation sequencing (ChIP-seq) at 120,387 peaks, 36,517 peaks, and 97,234 peaks, respectively.

Before focusing on locus-specific differences in our data, we first examined overall separation among the four groups of mice using unsupervised hierarchical clustering within each data set. Mice did not show clear clustering pattern by genotype or environment on examination by CpG methylation, CpH methylation, or CpH hydroxymethylation were examined (Fig. 2A, B, D). However, mice were separated by genotype in the CpG hydroxymethylation, H3K4me1, H3K4me3, and H3K27ac data sets, with the hydroxymethylation, H3K4me1, and H3K27ac genotype clusters stable under bootstrapping (AU (approximately unbiased) $p < 0.01$, `pvclust` R package; Fig. 2C, E-G) (Suzuki and Shimodaira, 2006). Using unsupervised principal component analysis, interindividual variation between the mice housed in EE was also apparent, particularly within DNAm and DNAhm (Fig. A.3). These observations indicated that genotype-related differences were most clearly discernible in the CpG hydroxymethylation, H3K4me1, and H3K27ac data, while environment-related differences were less apparent among all data sets.

3.2. SNCA overexpression induced changes in hippocampal DNAhm levels independently of the enriched environment

After assessing intersample clustering patterns, we conducted analyses of differential DNAm, DNAhm, and histone modification within each data set to elucidate the underlying locus-specific impacts of the *SNCA* transgene, the EE, and their interaction which drove the genotype

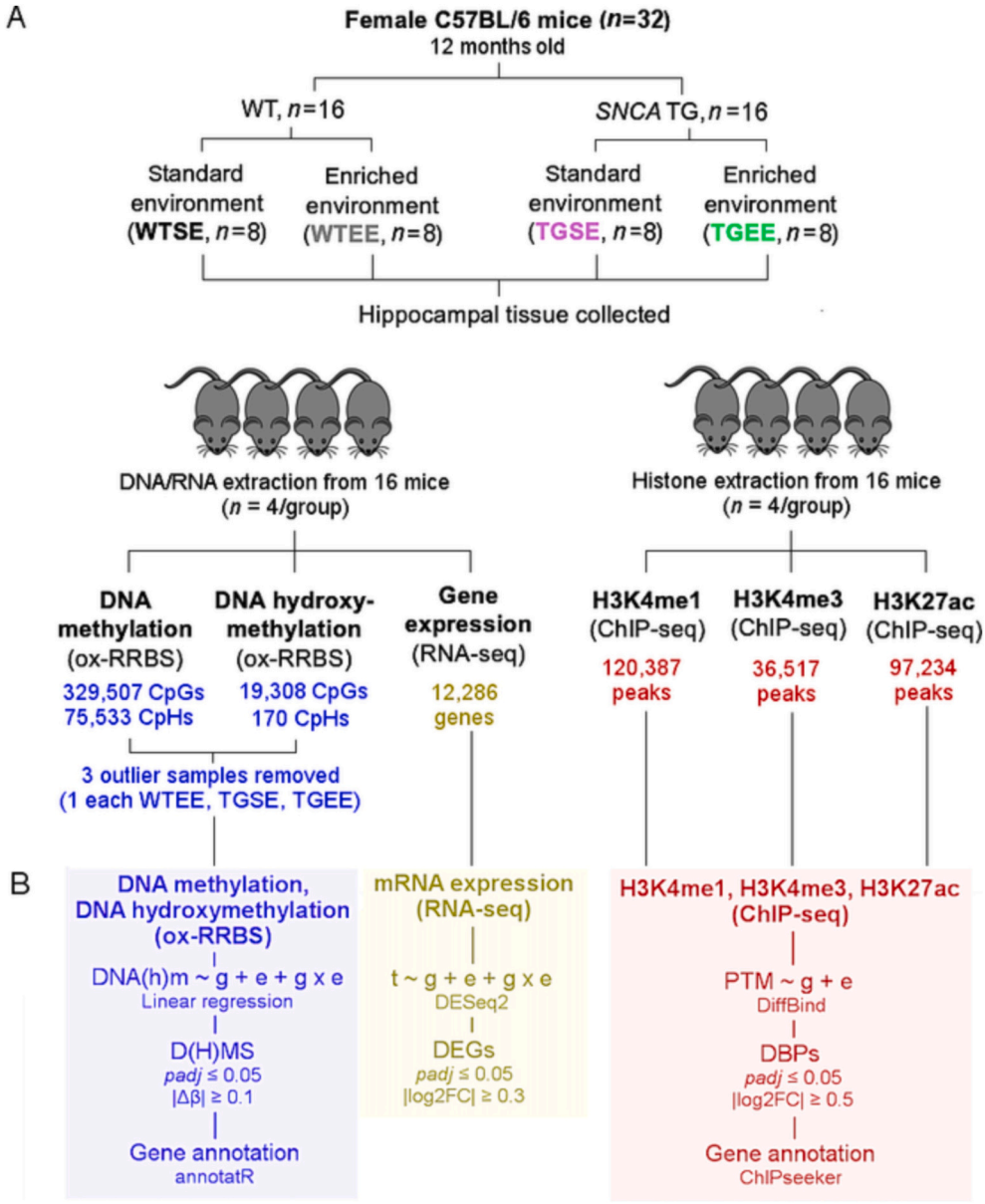

Fig. 1. Overview of experimental design and group comparison analysis within each data set. (A) Overview of the experimental design and sample collection. The numbers of cytosines, genes, or peaks retained after data QC and preprocessing are shown. Abbreviations: EE, enriched environment; ox-RRBS, oxidative reduced representation bisulfite sequencing; SE, standard environment; TG, *SNCA* transgenic; WT, wild-type. (B) Overview of differential analysis for DNAm, DNAhm, H3K4me1, H3K4me3, H3K27ac, and mRNA expression. D(*H*)MS: differentially (hydroxy)methylated site, DBP: differentially bound peak, DEG: differentially expressed gene, FC: fold change.

and genotype-environment interaction effects separating the four groups of mice in the unsupervised hierarchical clustering analysis (Fig. 2). In this approach, linear regression was used to assess differential DNAm and DNAhm separately at autosomal CpG and CpH sites (~ genotype + environment + genotype:environment; cytosines considered significant at $|\Delta\beta| \geq 0.1$ and $p_{adj} \leq 0.05$; Fig. 1B), and to assess differential H3K27ac, H3K4me1, and H3K4me3 at consensus peaks using the `DiffBind` R package, designed for pairwise comparisons between conditions (~ genotype + environment; peaks considered significant at $|\log2FC| \geq 0.5$ and $p_{adj} \leq 0.05$; Fig. 1B) (Stark and Brown, 2011). Differential mRNA expression was assessed previously with `DESeq2` (~ genotype + environment + genotype:environment; genes considered significant at |log2 fold change [FC]| ≥ 0.3 and $p_{adj} \leq 0.05$; Fig. 1B) (Wassouf et al., 2018; Love et al., 2014).

To examine DNAm changes associated with *SNCA* overexpression in either environment, we assessed DNAm at 329,507 autosomal CpG sites and 75,533 autosomal CpH sites present in all samples and passing QC and variability filtering. We observed only one differentially methylated CpG each ($|\Delta\beta| \geq 0.1$, $p_{adj} \leq 0.05$) in comparison of TG_{SE} and WT_{SE} mice (chr4: 72680131, located in an intergenic region; $\Delta\beta = -0.15$, $p_{adj} = 1.49 \times 10^{-6}$) and in comparison of TG_{EE} and WT_{EE} mice (chr11: 102189736, in an active promoter of the *G6pc3* gene; $\Delta\beta = 0.10$, $p_{adj} = 0.025$). No significant interaction effects were detected ($p_{adj} > 0.05$) in either TG vs. WT comparison, and no CpGs showed differential methylation by environment (all WT_{EE} vs. WT_{EE} and TG_{EE} vs. TG_{SE} $p_{adj} > 0.05$).

A slight increase in differential CpH methylation was observed in mice overexpressing *SNCA*, with 14 CpHs differentially methylated in the TG_{SE} vs. WT_{SE} comparison (mapping primarily to intergenic regions and CpG open seas, and covering the *Thsd7b*, *Ggnbp2*, and *Padi3* genes) and 28 CpHs differentially methylated in the TG_{EE} vs. WT_{EE} comparison mapping primarily to intergenic regions, introns, and CpG open seas, and covering nine genes including components and regulators of the cytoskeleton (*Lamc2, Rmdn2, Sorbs2*), E3 ubiquitin ligases (*Rnf144b, Rnf165, Zyg11a*), components of the NuRD histone deacetylase complex (*Mta3*, *Sall1*), and a long noncoding RNA (*4930594O21Rik*)) (Fig. 3A-B, Tables 1, 2). Six CpHs were differentially methylated in mice overexpressing *SNCA* in both environments, which was greater than expected by chance (Fig. 3C, $p_{adj} < 0.001$, 1000 permutations). In addition, a small number of CpHs were differentially methylated between mice of

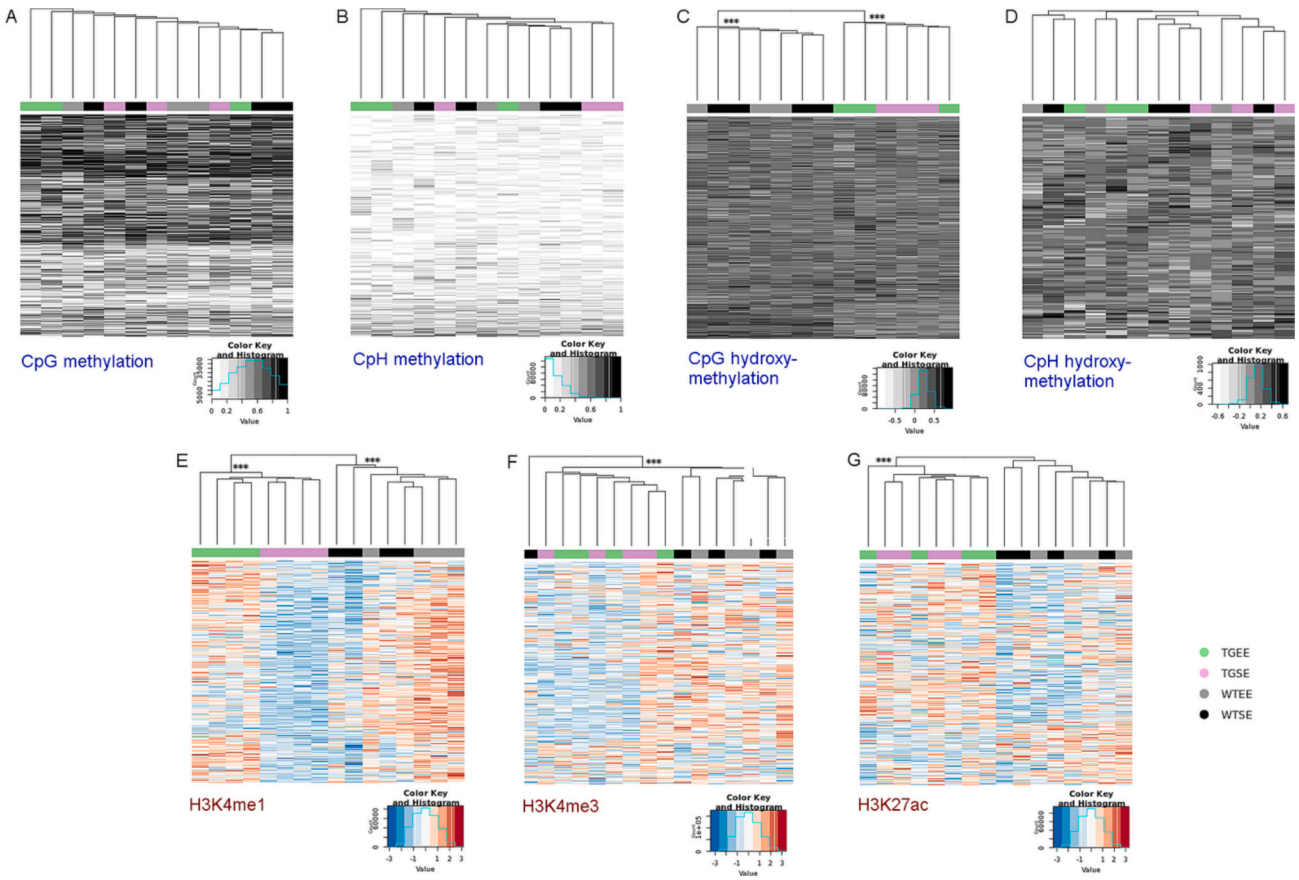

Fig. 2. Hippocampal CpG hydroxymethylation and histone post-translation modifications clustered by genotype in *SNCA* transgenic mice. Unsupervised hierarchical clustering of cytosines or peaks from each data set are shown. *** cluster $p < 0.01$ (*pvclust*). (A) Top 20,000 most variable CpGs (using IQR reference range) from the total 329,507 assessed for DNAm. Cell fill: β value. (B) Top 20,000 most variable CpHs from the total 75,533 assessed for DNAm. Cell fill: β value. (C) 19,308 CpGs assessed for DNAm. Cell fill: β value. (D) 170 CpHs assessed for DNAhm. Cell fill: β value. (E) Top 20,000 most variable peaks from the total 120,387 assessed for H3K4me1. Cell fill: *Z*-score. (F) 36,517 peaks assessed for H3K4me3. Cell fill: Z-score. (G) Top 20,000 most variable peaks from the total 97,234 assessed for H3K27ac. Cell fill: Z-score.

the same genotype housed in EE and SE ($|\Delta\beta| \geq 0.1$, $p_{adj} \leq 0.05$): six CpHs mapping to three genes (*94O21Rik, Zyg11a, Gm3134*) were significant in the WT_{EE} vs. WT_{SE} comparison, while nine CpHs mapping to six genes were significant in the TG_{EE} vs. TG_{SE} comparison, including three genes also differentially methylated in TG_{EE} vs. WT_{EE} mice (*Lamc2, Rnf144b, Rnf165*), one gene also differentially methylated in TG_{SE} vs. WT_{SE} mice (*Ggnbp2*), and two genes unique to this comparison (*Slc14a2* and *Mov10*) (Tables A.2, A.3). In summary, these results indicated that *SNCA* overexpression and EE each had little impact on CpG methylation and some impact on CpH methylation.

As CpH methylation is enriched in mammalian neurons relative to glia, we hypothesized that *SNCA* overexpression may also be associated with changes to DNAhm, another cytosine modification highly enriched in this cell type (Kinde et al., 2015). Based on the results of hierarchical clustering analysis, we expected that a higher proportion of CpG hydroxymethylation changes would be associated with *SNCA* overexpression in comparison with CpG methylation changes, and that these would be consistent within SE or EE, as WT and TG samples formed separate, stable clusters (Fig. 2C, $p < 0.01$). To test this hypothesis, we examined DNAhm differences between WT and TG mice at 19,308 autosomal CpG sites. Indeed, there was a mean reduction in CpG hydroxymethylation between WT and TG mice of 5.3% when genotypes were compared within the SE and of 4.9% when genotypes were compared within the EE ($p_{adj} < 2.2 \times 10^{-16}$, ANOVA) (Fig. 4A). Differential hydroxymethylation analysis at single loci corroborated this observation. In SE, 707 CpGs were differentially hydroxymethylated with *SNCA* overexpression, with 697 CpGs (99%) showing decreased DNAhm in TG mice, and 10 CpGs (1%) showing increased DNAhm in TG mice ($|\Delta\beta| \geq 0.1$, $p_{adj} \leq 0.05$, skewness $p < 2.2 \times 10^{-16}$) (Fig. 4B, Fig. A.4). Application of overrepresentation analysis to the genes mapping to these differentially hydroxymethylated CpGs (using all genes covered by the 19,308 variable CpGs tested for differential hydroxymethylation as background) showed enrichment for the GO Cellular Component term "extracellular space" ($p_{adj} = 0.04$). We also calculated the enrichment of differentially hydroxymethylated CpGs for genes expressed in five hippocampal cell types (interneurons, pyramidal neurons, oligodendrocytes, microglia, and astrocytes), using single-cell RNA-seq data from the mouse hippocampus (Zeisel et al., 2015). CpGs with loss of DNAhm in TG_{SE} mice mapped to fewer genes expressed in oligodendrocytes than expected by chance, consistent with known enrichment of DNAhm in neurons relative to glia ($p_{adj} = 0.03$, Fig. A.6A).

On comparison of TG_{EE} and WT_{EE} mice, fewer CpGs passed the thresholds for differential hydroxymethylation, although hydroxymethylation levels were similar within each genotype when visualized on heat maps (Fig. 4C). A total of 370 CpGs were differentially hydroxymethylated in the TG_{EE} vs. WT_{EE} comparison, with 366 CpGs (99%) showing decreased DNAhm and 4 CpGs (1%) showing increased DNAhm in TG mice (skewness $p < 2.2 \times 10^{-16}$; no GO enrichment at $p_{adj} \leq 0.05$) (Fig. 4C, Fig. A.5). A greater proportion of the total differentially hydroxymethylated CpGs were significant in both comparisons than expected by chance (248, 30%), with 247 showing decreased DNAhm in TG mice in both SE and EE (Fig. 4D, enrichment $p_{adj} < 0.001$, 1000 permutations). The CpGs with reduced DNAhm in both comparisons were enriched for exons and intergenic regions, and depleted for active

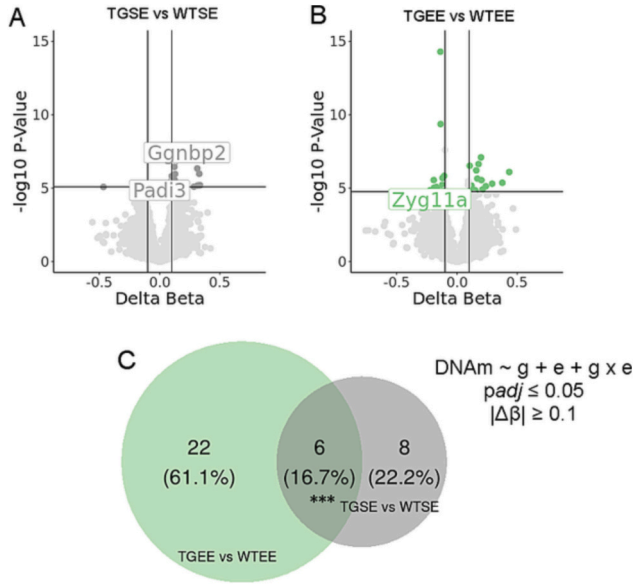

Fig. 3. Differential CpH methylation in the TG_{SE} vs. WT_{SE} and TG_{EE} vs. WT_{EE} comparisons. (A) Volcano plot showing differentially methylated CpHs in the TG_{SE} vs. WT_{SE} comparison. Dark gray points passed thresholds of $|\Delta\beta| \geq 0.1$ and $p_{adj} \leq 0.05$. (B) Volcano plot showing differentially methylated CpHs in the TG_{EE} vs. WT_{EE} comparison. Green points passed thresholds of $|\Delta\beta| \geq 0.1$ and $p_{adj} \leq 0.05$. (C) Overlap in differentially methylated CpHs between the TG_{EE} vs. WT_{EE} (green) and TG_{SE} vs. WT_{SE} (gray) comparisons. *** $p_{adj} < 0.001$ (1000 permutations). (For interpretation of the references to color in this figure legend, the reader is referred to the web version of this article.)

Table 1
Differentially Methylated CpHs in TG_{SE} vs. WT_{SE} Mice ($|\Delta\beta| \geq 0.1$, $p_{adj} \leq 0.05$).

Coordinate	Gene	Gene feature	CpG island feature	Δβ	p_{adj}
chr1: 129768011	*Thsd7b*	Intron	Open sea	0.28	0.045
chr1: 177421430	n/a	Intergenic	Open sea	0.12	0.033
chr10: 65938345	n/a	Intergenic	Open sea	0.33	0.021
chr11: 84870406	*Ggnbp2*	Active promoter	CpG island	0.12	0.017
chr13: 99788771	n/a	Intergenic	Open sea	0.31	0.017
chr13: 113707658	n/a	Intergenic	Open sea	0.12	0.030
chr14: 53929892	n/a	Intergenic	Open sea	0.34	0.042
chr18: 51073430	n/a	Intergenic	Open sea	0.12	0.030
chr2: 75586418	n/a	Intergenic	Open sea	−0.14	0.041
chr4: 135109966	n/a	Intergenic	Open sea	0.12	0.041
chr4: 140795682	*Padi3*	Exon–intron boundary	Open sea	0.10	0.023
chr6: 15971331	n/a	Intergenic	Open sea	0.32	0.042
chr6: 16966299	n/a	Intergenic	Open sea	0.13	0.021
chr7: 119439963	n/a	Intergenic	Open sea	−0.47	0.045

Coordinates are based on the mm10 reference genome.
p_{adj}, Benjamini–Hochberg adjusted *p*-value.

enhancers, promoters, and genes expressed in oligodendrocytes (enrichment/depletion $p_{adj} < 0.05$, 1000 permutations) (Fig. 4D, Figs. A.4-A.6). In addition, no differences in CpG hydroxymethylation were detected at the same statistical thresholds in comparisons of WT_{EE} and WT_{SE} or TG_{EE} and TG_{SE} mice, and no interaction effects were detected in any of the pairwise comparisons, suggesting that genotype was the major driver of between-group differences in DNAhm.

Finally, we examined CpH hydroxymethylation at 170 cytosines passing QC and variability filters. No differences were detected in either of the genotype or environment pairwise comparisons, consistent with the low level of hydroxymethylated CpHs in the mammalian brain (~1% of cytosines in the adult mouse cortex) and with the lack of a clear genotype or environment separation pattern in hierarchical clustering analysis (Fig. 2D) (Lister et al., 2013).

3.3. H3K27ac changes associated with SNCA overexpression were primarily consistent between environments

The presence or absence of DNAhm may be associated with H3K27ac level, as MeCP2 can bind hydroxymethylated DNA and recruit histone deacetylases (Kinde et al., 2015; Mellén et al., 2012). Similar to DNAhm, mice separated by genotype when clustered by H3K27ac level, suggesting possible changes in H3K27ac associated with *SNCA* overexpression independent of the environment (Fig. 2G). Differential H3K27ac enrichment analysis supported a strong impact of *SNCA* genotype on H3K27ac levels within both environments (1152 differentially acetylated peaks comparing TG_{SE} and WT_{SE} mice, 1191 differentially acetylated peaks comparing TG_{EE} and WT_{EE} mice, $|\log2FC| \geq 0.5$ and $p_{adj} \leq 0.05$, Fig. 5), and a lack of impact of EE on H3K27ac (all WT_{EE} vs. WT_{SE} and TG_{EE} vs. TG_{SE} $p_{adj} > 0.05$). The majority of differentially acetylated peaks had increased H3K27ac associated with *SNCA* overexpression (66% of peaks in the SE comparison, 61% of peaks in the EE comparison), and a greater number of peaks were differentially acetylated in both environments than expected by chance (160 peaks, 7% of total; enrichment $p_{adj} < 0.001$, 1000 permutations) (Fig. 5E). In addition, H3K27ac levels were similar between WT and TG mice even when these group differences only met thresholds in one environment (Fig. 5B, D).

Peaks with differential H3K27ac in either the WT_{SE} vs. TG_{SE} or the WT_{EE} vs. TG_{EE} comparisons were enriched for intergenic regions and depleted for enhancers, similar to DNAhm; however, unlike DNAhm, H3K27ac changes were also enriched at promoters and introns (Fig. 5A, D). Enrichment analysis for GO terms and hippocampal cell types also indicated similarity between effects of *SNCA* overexpression on H3K27ac in each environment at cell signaling-related genes and genes expressed in pyramidal neurons ($p_{adj} \leq 0.05$, Figs. A.7, A.8).

Despite these similarities in differential H3K27ac associated with *SNCA* overexpression, there were also subtle differences between peak sets passing statistical thresholds in each environment. Differentially acetylated peaks with both loss and gain of H3K27ac in SE were enriched for neurogenesis and cell adhesion pathways, while peaks with loss of H3K27ac in SE were additionally enriched for expression in oligodendrocytes and depleted for expression in microglia ($p_{adj} \leq 0.05$, Fig. A.7). Conversely, differentially acetylated genes in EE were enriched for transmembrane transport pathways (Fig. A.8). Taken together, these results indicated that DNAhm and H3K27ac were both altered at gene bodies in a manner primarily dependent on *SNCA* overexpression, with some subtle differences related to the environment, and that H3K27ac changes impacted pathways previously shown to be associated with functions of aSyn.

Next, to determine the functional relevance of these *SNCA*-dependent changes in CpG hydroxymethylation and H3K27ac, we assessed the number of differentially expressed genes (DEGs) containing one or more differentially hydroxymethylated CpGs and/or differentially acetylated peaks at any genomic locus. Only a small number of the 215 DEGs in the TG_{SE} vs. WT_{SE} comparison had H3K27ac changes (6 genes, 3% of total) (Table A.4), and none had changes in DNAhm. None of the three DEGs in the TG_{EE} vs. WT_{EE} comparison had a change in H3K27ac or DNAhm. The overlap between differential expression and differential H3K27ac was

Table 2
Differentially Methylated CpHs in TG_{EE} vs. WT_{EE} Mice ($|\Delta\beta| \geq 0.1$, $p_{adj} \leq 0.05$).

Coordinate	Gene	Gene feature	CpG island feature	Δβ	p_{adj}
chr1: 153170229	*Lamc2*	Intron	Open sea	0.11	0.004
chr1: 177421430	n/a	Intergenic	Open sea	0.12	0.027
chr1: 189061453	n/a	Intergenic	Open sea	−0.11	0.012
chr10: 65938345	n/a	Intergenic	Open sea	0.29	0.024
chr11: 10627542	n/a	Intergenic	Open sea	−0.12	0.015
chr11: 41000752	n/a	Intergenic	Open sea	0.18	0.003
chr11: 54038139	n/a	Intergenic	Open sea	−0.14	3.85E−10
chr12: 47865685	n/a	Intergenic	Open sea	0.21	0.038
chr12: 92713716	n/a	Intergenic	Open sea	−0.14	0.041
chr13: 47215999	*Rnf144b*	Intron	Open sea	0.11	0.038
chr13: 99788771	n/a	Intergenic	Open sea	0.24	0.028
chr14: 53929892	n/a	Intergenic	Open sea	0.38	0.022
chr16: 19119960	n/a	Intergenic	Open sea	0.15	0.038
chr16: 30774432	n/a	Intergenic	Open sea	−0.16	0.041
chr17: 79618749	*Rmdn2*	Intron	CpG shelf	0.17	0.015
chr17: 83773055	*Mta3*	Intron	Open sea	0.12	0.038
chr18: 51073430	n/a	Intergenic	Open sea	0.20	0.002
chr18: 77515699	*Rnf165*	Intron	Open sea	0.16	0.007
chr19: 56197768	n/a	Intergenic	Open sea	−0.19	0.032
chr2: 160583325	*Gm14221*	Promoter	Open sea	−0.30	0.050
chr3: 9301399	n/a	Intergenic	Open sea	0.13	0.038
chr3: 37613773	*4930594O21Rik*	Promoter	Open sea	−0.17	0.030
chr3: 133555760	n/a	Intergenic	Open sea	−0.22	0.038
chr4: 108217654	*Zyg11a*	Exon–intron boundary	CpG island	−0.12	0.026
chr5: 71342562	n/a	Intergenic	Open sea	−0.19	0.017
chr6: 15971331	n/a	Intergenic	Open sea	0.43	0.008
chr7: 111813638	n/a	Active enhancer	Open sea	0.20	0.017
chr8: 45819257	*Sorbs2*	Intron	Open sea	−0.11	0.041
chr8: 89044885	*Sall1*	Active promoter	CpG shore	−0.14	1.63E−05

Coordinates are based on the mm10 reference genome.
p_{adj}, Benjamini–Hochberg adjusted *p*-value.
n/a: not applicable.

no greater than expected by chance (enrichment $p_{adj} = 1$, 1000 permutations). This indicated that additional factors were likely involved in transcription regulation in these mice.

3.4. H3K4me1 alterations associated with SNCA overexpression were modulated by environmental enrichment

In addition to DNAhm and H3K7ac, H3K4 methylation also plays a role in transcriptional regulation and may contribute to the molecular phenotype associated with excess hippocampal aSyn. Specifically, H3K4me1 is found at enhancers and may fine-tune levels of gene expression, while H3K4me3 is associated with promoters of actively transcribed genes (Rada-Iglesias, 2018; Kimura, 2013). The results of hierarchical clustering analysis showed that *SNCA* genotype was associated with H3K4 methylation pattern, which was also supported by differential H3K4me1 enrichment analysis (Fig. 2E). However, H3K4me1 patterns differed slightly in association with *SNCA* overexpression depending on whether mice were housed in SE or EE (Figs. 6, 7A-C).

Comparison of TG_{SE} and WT_{SE} mice primarily revealed loss of H3K4me1 (3878 peaks [84%] with H3K4me1 loss; 763 peaks [16%] with H3K4me1 gain; $|\log2FC| \geq 0.5$ and $p_{adj} \leq 0.05$) (Fig. 6A–C). The peaks with altered H3K4me1 were enriched for exons and introns, and depleted for promoters and enhancers, similar to trends seen in the levels of DNAhm and H3K27ac (Fig. 6A). Genes with altered H3K4me1 were enriched for neurodevelopment-related GO terms, including "neurogenesis" and "neuron differentiation," and for genes expressed in pyramidal neurons, and were depleted for genes expressed in microglia (Fig. 6B, Fig. A.9A). Unlike the trends observed for DNAhm and H3K27ac, this loss of H3K4me1 in TG_{SE} mice did not occur to the same magnitude in TG_{EE} mice at the same peaks (Fig. 6C). However, no peaks passed statistical significance when comparing WT_{EE} and WT_{SE} or TG_{EE} and TG_{SE} mice ($p_{adj} > 0.05$), suggesting the impact of genotype was much greater than the impact of the environment on hippocampal H3K4me1 patterns, with detection of some subtle gene–environment interaction effects.

The H3K4me1 alterations observed in the context of SE co-occurred with changes in other epigenetic marks and in gene expression. For example, 455 genes showed altered H3K4me1 and H3K27ac levels in the TG_{SE} vs. WT_{SE} comparison, which was greater than expected by chance ($p_{adj} < 0.001$, 1000 permutations) (Fig. 6D). Genes with altered H3K4me1 and H3K27ac in the context of SE were enriched for "synapse organization" and "locomotion" GO Biological Process terms, pathways which were not identified when each histone PTM was analyzed separately (Fig. A.10). In addition, the overlap between H3K4me1, H3K27ac, and DNAhm changes at four genes was greater than expected by chance, affecting loci encoding a protein with protease and ER-Golgi transport functions (*Adamts20*), a voltage-gated calcium channel (*Cacna1c*), a voltage-gated potassium channel (*Kcnq2*), and a type IV collagen alpha protein (*Col4a1*) ($p_{adj} < 0.05$, 1000 permutations) (Fig. 6D, Table B.1). Finally, 34 genes had altered H3K4me1 and mRNA expression in the TG_{SE} vs. WT_{SE} comparison, a rate greater than expected by chance (16% of total DEGs, enrichment $p_{adj} < 0.05$, 1000 permutations) (Fig. 6D, E, Table A.5). This group of genes included cell signaling proteins (*Acvr2a*, *Neurl1b*, *Rps6ka2*) and transcription factors (*Glis2*, *Hivep1*, *Per1*, *Zfhx2*) involved in neurodevelopment, as well as components of the cytoskeleton (*Flnb*, *Lrch3*, *Tns1*, *Tnxb*), calcium-binding proteins (*Cacna1i*, *Fat4*, *Heg1*, *Hpcal1*, *Otof*), and a spliceosome component differentially spliced in blood and brain of patients with PD (*Srrm2*; Table A.5) (Shehadeh et al., 2010). Examination of mice across all four groups revealed similarities between enhancer/promoter/intron H3K4me1 levels and mRNA expression levels, which were apparent across the majority of these 34 genes, including *Per1* (Fig. 6D, E, Table A.5). Taken together, these results indicated that the EE could dampen changes to H3K4me1, either alone or in combination with other epigenetic changes induced by expression of the *SNCA* transgene.

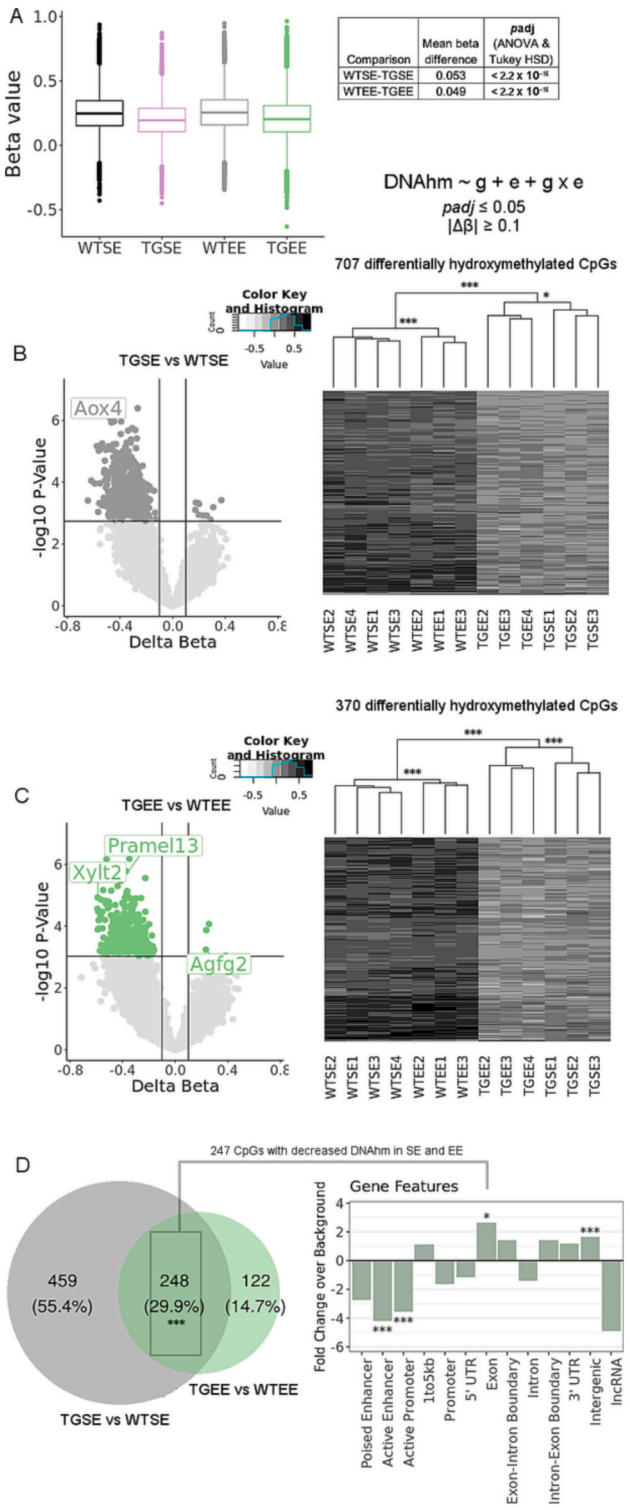

Fig. 4. DNAhm loss in *SNCA* transgenic mice was consistent across environments. (A) β values across 19,308 CpGs tested for differential hydroxymethylation. (B) Volcano plot (left) and heat map (right) showing CpGs differentially hydroxymethylated at $p_{adj} \leq 0.05$ and $|\Delta\beta| \geq 0.1$ in TG_{SE} vs. WT_{SE} comparison (significant CpGs indicated in gray). β values are shown on a continuous color scale where white indicates low/no DNAhm and black indicates high DNAhm. (C) Volcano plot (left) and heat map (right) showing CpGs differentially hydroxymethylated at $p_{adj} \leq 0.05$ and $|\Delta\beta| \geq 0.1$ in TG_{EE} vs. WT_{EE} comparison (significant CpGs shown in green). (D) Enrichment/depletion of DNAhm loss at 247 CpGs in TG_{SE} and TG_{EE} mice across gene features. *** $p_{adj} <$ 0.001 (1000 permutations). (For interpretation of the references to color in this figure legend, the reader is referred to the web version of this article.)

3.5. Environmental enrichment increased the divergence in H3K4me1 and H3K4me3 levels between wild-type and SNCA-overexpressing mice

We hypothesized that there would be overall similarity between differential H3K4me1 patterns associated with *SNCA* overexpression in either environment, similar to the other epigenetic marks assessed in this study, as genotypes clustered together (Fig. 2E). In comparison of TG_{EE} with WT_{EE} mice, the overall reduction in H3K4me1 level associated with *SNCA* overexpression across many of the same peaks identified in SE was still present, impacting similar genes and gene features as when mice were housed in SE (3346 peaks [66%] with H3K4me1 loss, 1657 peaks [33%] with H3K4me1 gain; $|\log2FC| \geq 0.5$ and $p_{adj} \leq 0.05$) (Fig. 7A–C, Fig. A.11A-B). A greater proportion of peaks showed differential H3K4me1 in both SE and EE than expected by chance, most of which had reduced H3K4me1 (1039 peaks [12% of total]; 862 with decreased H3K4me1; $p_{adj} < 0.001$, 1000 permutations) (Fig. 7A). Similar to peaks with differential H3K4me1 in the SE comparison, peaks with differential H3K4me1 in the EE comparison were enriched for genes expressed in pyramidal neurons and depleted for genes expressed in microglia (Fig. A.9B).

In addition to this overall similarity in *SNCA*-associated differential H3K4me1 patterns between environments, we also found evidence supporting a gene–environment interaction effect. TG_{SE} and TG_{EE} mice clustered separately from each other when examining the top 20,000 most variable H3K4me1 peaks, although we note that this clustering was not statistically significant (Fig. 2E). When H3K4me1 levels at peaks differentially enriched in the TG_{EE} vs. WT_{EE} comparison were plotted in all four groups, two groups of peaks showing distinct differential H3K4me1 patterns were evident. While the EE did not affect H3K4me1 levels in TG mice at peaks with *SNCA*-associated H3K4me1 loss, it was associated with increased H3K4me1 levels in WT mice, making the combined effects of *SNCA* overexpression and EE detectable even though the effects of EE alone did not pass statistical significance in the WT_{EE} vs. WT_{SE} comparison (Fig. 7B). Conversely, the combination of the *SNCA* transgene and EE resulted in H3K4me1 gain for a different subset of peaks (Fig. 7B). These peaks with increased H3K4me1 in TG_{EE} mice were depleted for genes expressed in interneurons, an effect not seen in TG_{SE} mice ($p = 0.006$, Fig. A.9B). These observations indicated that *SNCA* overexpression facilitated EE-dependent increases to H3K4me1 levels at some peaks, while other peaks were resistant to the effects of EE in TG mice.

We also observed some gene–environment interaction effects of EE and aSyn on H3K4me3 levels. Similar to H3K4me1, the EE had unique impacts on H3K4me3 levels in WT mice, which were not seen in TG mice (Fig. 7D,E). *SNCA* overexpression had a greater impact on mice in the context of EE than in the context of SE, preventing the EE-dependent increases in H3K4me3 observed in WT mice at genes related to transcriptional and metabolic regulation (201 differentially bound peaks in TG_{EE} vs. WT_{EE} mice, 9 differentially bound peaks in TG_{SE} vs. WT_{SE} mice; $|\log2FC| \geq 0.5$ and $p_{adj} \leq 0.05$) (Fig. 7D-E, Fig. A.11, A.12). As with H3K27ac and H3K4me1, these H3K4me3 changes were enriched at introns and depleted from active promoters ($p_{adj} < 0.05$, 1000 permutations), and similar to H3K4me1, H3K4me3 peaks were depleted for genes expressed in interneurons (Fig. A.11D, A.13). There were no statistically significant differences in H3K4me3 in the WT_{EE} vs. WT_{SE} or TG_{EE} vs. TG_{SE} comparisons ($p_{adj} > 0.05$). In summary, *SNCA* transgene expression consistently decreased gene body H3K4me1 and H3K4me3 levels, while housing mice in EE increased gene body H3K4me1 and H3K4me3 levels in a manner dependent on genotype.

Finally, we examined the overlap between genotype-dependent changes in H3K4 methylation associated with housing mice in EE and changes to the other epigenetic marks observed when mice were housed under the same conditions. H3K4 methylation changes associated with *SNCA* overexpression in EE tended to occur alongside changes in H3K27ac (473 genes with altered H3K4me1 and H3K27ac; nine genes with altered H3K4me1, H3K4me3, and H3K27ac) and/or DNAhm (four

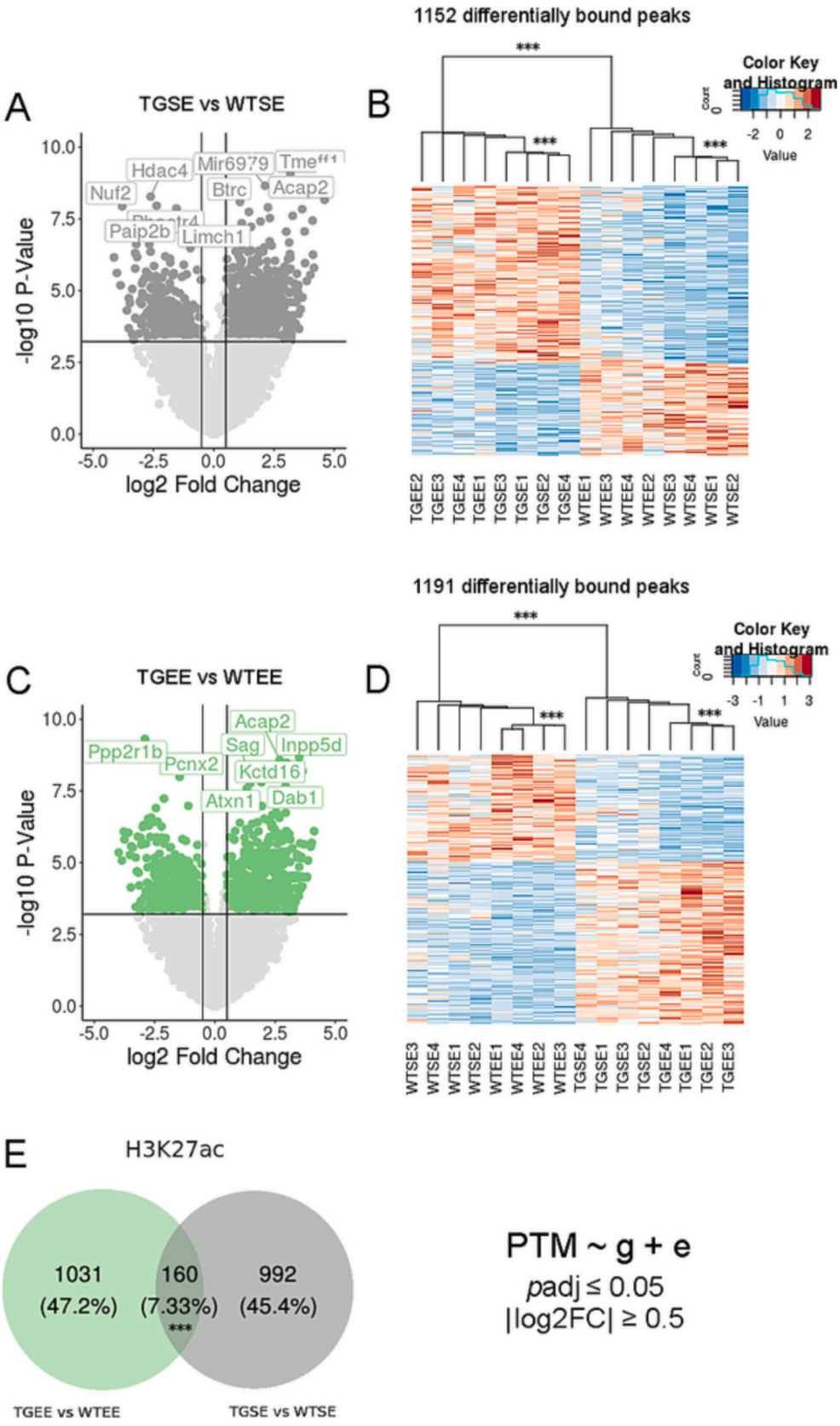

Fig. 5. *SNCA* overexpression altered genome-wide H3K27ac levels in standard and enriched environments. (A) Volcano plot showing differentially bound H3K27ac peaks in the TG_{SE} vs. WT_{SE} comparison. Dark gray colored points passed thresholds of $|log2FC| \geq 0.5$ and $p_{adj} \leq 0.05$. (B) Row *Z*-scores for mean H3K27ac levels within each group at 1152 peaks differentially bound in the TG_{SE} vs. WT_{SE} comparison, displayed on a diverging color scale to indicate negative versus positive Z-score values. Blue, low H3K27ac; red, high H3K27ac. (C) Volcano plot showing differentially bound H3K27ac peaks in the TG_{EE} vs. WT_{EE} comparison. Green colored points passed thresholds of $|log2FC| \geq 0.5$ and $p_{adj} \leq 0.05$. (D) Row Z-scores for mean H3K27ac levels within each group at 1191 peaks differentially bound in the TG_{EE} vs. WT_{EE} comparison. Blue, low H3K27ac; red, high H3K27ac. (E) Overlap in differentially bound peaks between TG_{SE} vs. WT_{SE} and TG_{EE} vs. WT_{SE} comparisons. *** $p_{adj} < 0.001$ (1000 permutations). (For interpretation of the references to color in this figure legend, the reader is referred to the web version of this article.)

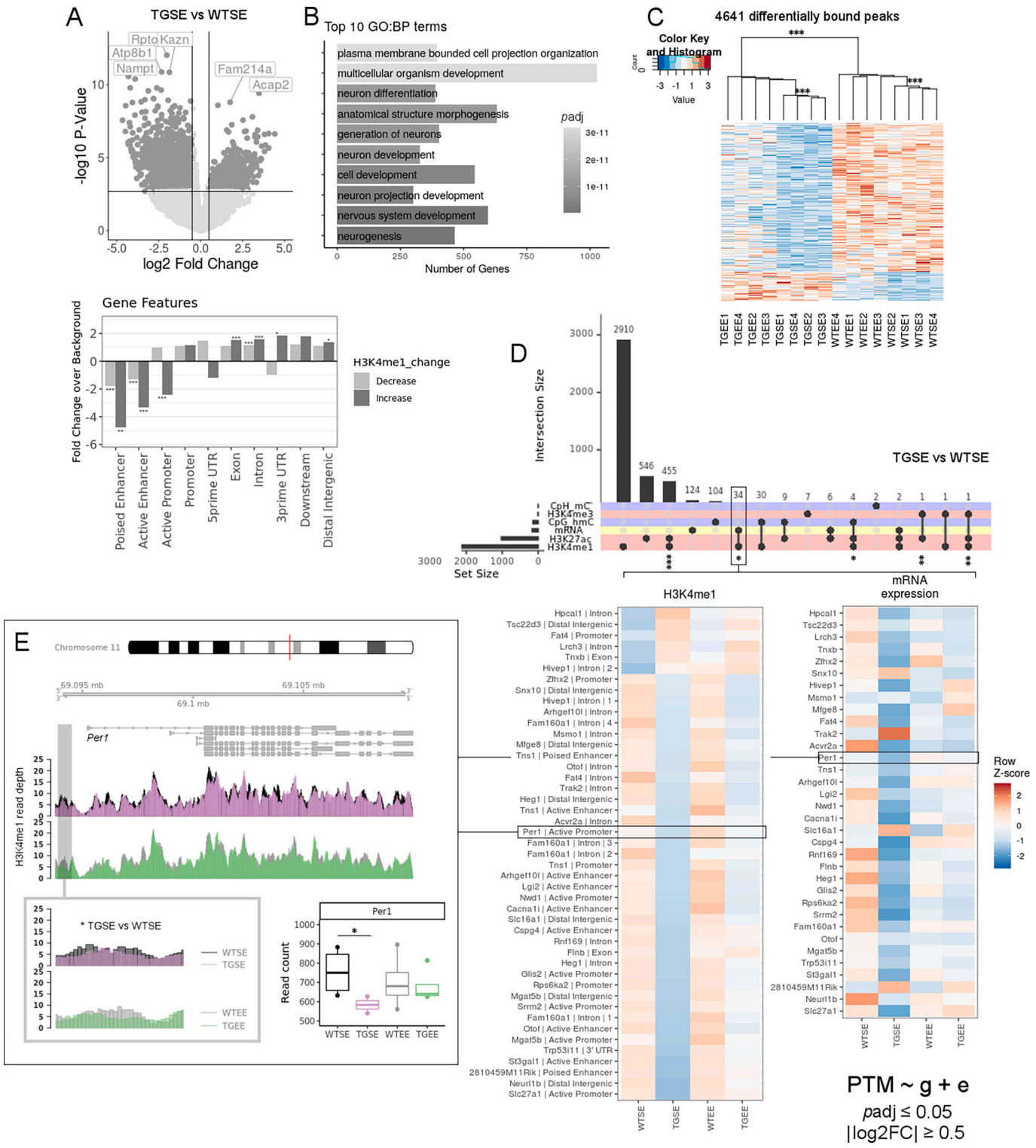

Fig. 6. *SNCA* overexpression induced H3K4me1 loss in the context of SE, which was partially dampened by EE. (A) Top: Volcano plot showing differentially bound H3K4me1 peaks in the TG_{SE} vs. WT_{SE} comparison. Dark gray points passed thresholds of $|log2FC| \geq 0.5$ and $p_{adj} \leq 0.05$. Bottom: Enrichment/depletion of H3K4me1 changes across gene features. (B) Top 10 GO Biological Process terms enriched in genes with differential H3K4me1 in the TG_{SE} vs. WT_{SE} comparison, ranked by significance. Darker color indicates lower *p*-value. (C) Row *Z*-scores for mean H3K4me1 levels within each group at 4641 peaks differentially bound in the TG_{SE} vs. WT_{SE} comparison, shown on a diverging color scale indicating negative vs. positive Z-score values. Blue, low H3K4me1; red, high H3K4me1. (D) Top: Overlap of differentially expressed genes, differentially methylated/hydroxymethylated genes, and differentially bound genes for the TG_{SE} vs. WT_{SE} comparison. Bottom: Row Z-scores for H3K4me1 and mRNA expression levels at 34 genes with significant differential H3K4me1 and mRNA expression in SE. Red, low H3K4me1/expression; blue, high H3K4me1/expression. (E) *Per1* is shown as an example of a gene with differential H3K4me1 and mRNA expression. Normalized H3K4me1 read depth for differentially bound *Per1* peak (left), and normalized mRNA expression read counts for *Per1* (right) are shown. * $p_{adj} < 0.05$, ** $p_{adj} < 0.01$, *** $p_{adj} < 0.001$. (For interpretation of the references to color in this figure legend, the reader is referred to the web version of this article.)

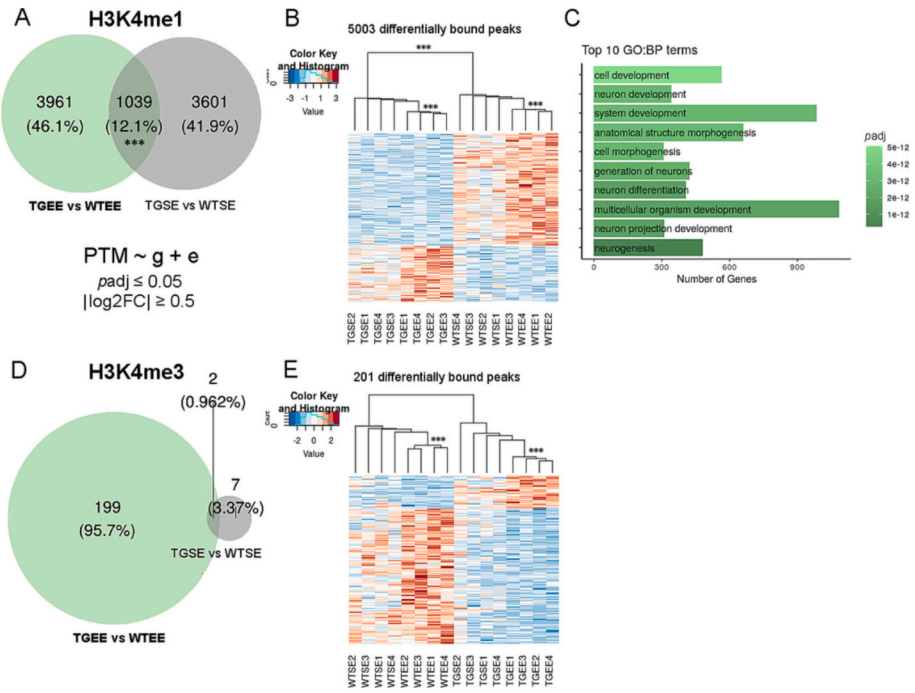

Fig. 7. A subset of loci had no environment-dependent changes to H3K4me1 or H3K4me3 in *SNCA* transgenic mice. (A) Overlap between H3K4me1 peaks differentially bound in the TG_{EE} vs. WT_{EE} comparison (green) and/or the TG_{SE} vs. WT_{SE} comparison (gray). (B) Row *Z*-scores for mean H3K4me1 levels within each group at 5003 peaks differentially bound in the TG_{EE} vs. WT_{EE} comparison (blue, low H3K4me1; red, high H3K4me1). (C) Top 10 GO Biological Process terms enriched in genes with differential H3K4me1 in the TG_{EE} vs. WT_{EE} comparison, ranked by significance. Darker color indicates lower *p*-value. (D) Overlap between H3K4me3 peaks differentially bound in the TG_{EE} vs. WT_{EE} comparison (green) and/or the TG_{SE} vs. WT_{SE} comparison (gray). (E) Row Z-scores for mean H3K4me3 levels within each group at 201 peaks differentially bound in the TG_{EE} vs. WT_{EE} comparison (blue, low H3K4me3; red, high H3K4me3).

genes with altered H3K4me1, H3K27ac, and DNAhm; enrichment $p_{adj} <$ 0.001 for all stated overlaps, 1000 permutations), which were consistent with *SNCA* overexpression in both environments (Fig. 8, Tables B.2, B.3). However, the genes with H3K4 methylation and H3K27ac or DNAhm changes in the context of EE included transcriptional regulators (*Nfib*, *Chd7*, *Foxk1*, and *Arid5b*) as well as genes regulating metabolic (*Ndst1*, *Pi4ka*) and cell survival (*Pim3*) pathways (Tables B.2, B.3). These observations indicated that there was an additional layer of epigenetic regulation when *SNCA*-overexpressing mice were housed in EE comprised of both *SNCA*-dependent changes to DNAhm and H3K27ac and *SNCA*- and environment-dependent changes to H3K4 methylation, the latter of which showed greater overlap with DEGs.

4. Discussion

To understand how *SNCA* copy number variants impact susceptibility to PD and other synucleinopathies, and the degree to which these risks are malleable, it is important to examine the molecular underpinnings of excess aSyn in different environmental contexts. Here, we housed WT and *SNCA* TG mice in either an SE or EE paradigm, and investigated gene- and environment-dependent effects on two DNA modifications and three histone PTMs in the hippocampus. Overall, *SNCA* overexpression had a greater impact than the environment on molecular epigenetic variation in the hippocampus. However, the environment influenced specific *SNCA*-associated epigenetic changes in the levels of CpH methylation, H3K4me1, and H3K4me3. The altered DNA and histone modifications in *SNCA* TG mice observed in this study were consistent with previously reported effects of aSyn on expression of adhesion-related genes, endoplasmic reticulum (ER) stress susceptibility, DNA damage, and epigenetic regulation of glutamate signaling genes, and suggested that epigenomic deregulation was part of the molecular phenotype associated with excess aSyn (Schaffner et al., 2022; Paiva et al., 2017; Paiva et al., 2018). Our results also suggested that the impacts of excess aSyn and EE on the hippocampal epigenome interacted with each other, with aSyn either facilitating or preventing environment-associated epigenetic alterations.

4.1. Associations of aSyn with synaptic function, cell signaling, and epigenetic modifiers

We observed altered H3K27ac and H3K4me1 in genes related to synapse organization, neuronal differentiation, neurogenesis, and cell signaling in TG mice housed in SE, as well as joint alterations to H3K4me1 and gene expression in genes related to calcium signaling and transcriptional regulation, which are also involved in synaptic transmission and plasticity. These findings were consistent with our previous study in which we proposed that transcriptional alterations associated with *SNCA* overexpression could be related to disrupted synaptic function and activity-dependent signaling (Wassouf et al., 2018). Similarly, excess WT aSyn has been reported to impair neuronal differentiation and activity in PD patient-derived *SNCA* triplication-induced pluripotent stem cells, and aSyn was shown to contribute to neuronal differentiation through Ras activation and ERK/MAPK signaling (Oliveira et al., 2015; Chen et al., 2013). Taken together, the detected epigenetic alterations associated with *SNCA* overexpression could be related, at least in part, to the synaptic dysfunction associated with excess aSyn protein levels.

In addition to the possible indirect effects of aSyn on synaptic function and cell signaling, the changes in DNA(h)m and histone modifications observed in TG mice housed in both environments may have resulted from direct impacts of aSyn on epigenetic modifiers. For example, nuclear aSyn was shown to inhibit p300 in cell culture experiments using human- and rat-derived neurons and to be associated with reduced H3 acetylation (Jin et al., 2011; Kontopoulos et al., 2006). Consistent with our findings, aSyn levels were reported to be associated with altered sirutin and p300 activity as well as increased H3K27ac in bulk postmortem brain tissue from PD patients (Toker et al., 2021). Similarly, enhancer DNAhm levels are increased in PD patient-derived prefrontal cortex neurons, which was proposed to be related to *Tet2* mRNA upregulation and neuroinflammation (Marshall et al., 2020). However, there were no significant changes to *Tet* family transcripts in the RNA-seq data from the mice profiled in the present study, suggesting that our results may have reflected changes in Tet activity or other mechanisms of passive or active CpG oxidation, or that factors such as cell type heterogeneity may have masked possible cell type-specific changes in *Tet* expression (Wassouf et al., 2018; Marshall et al., 2020).

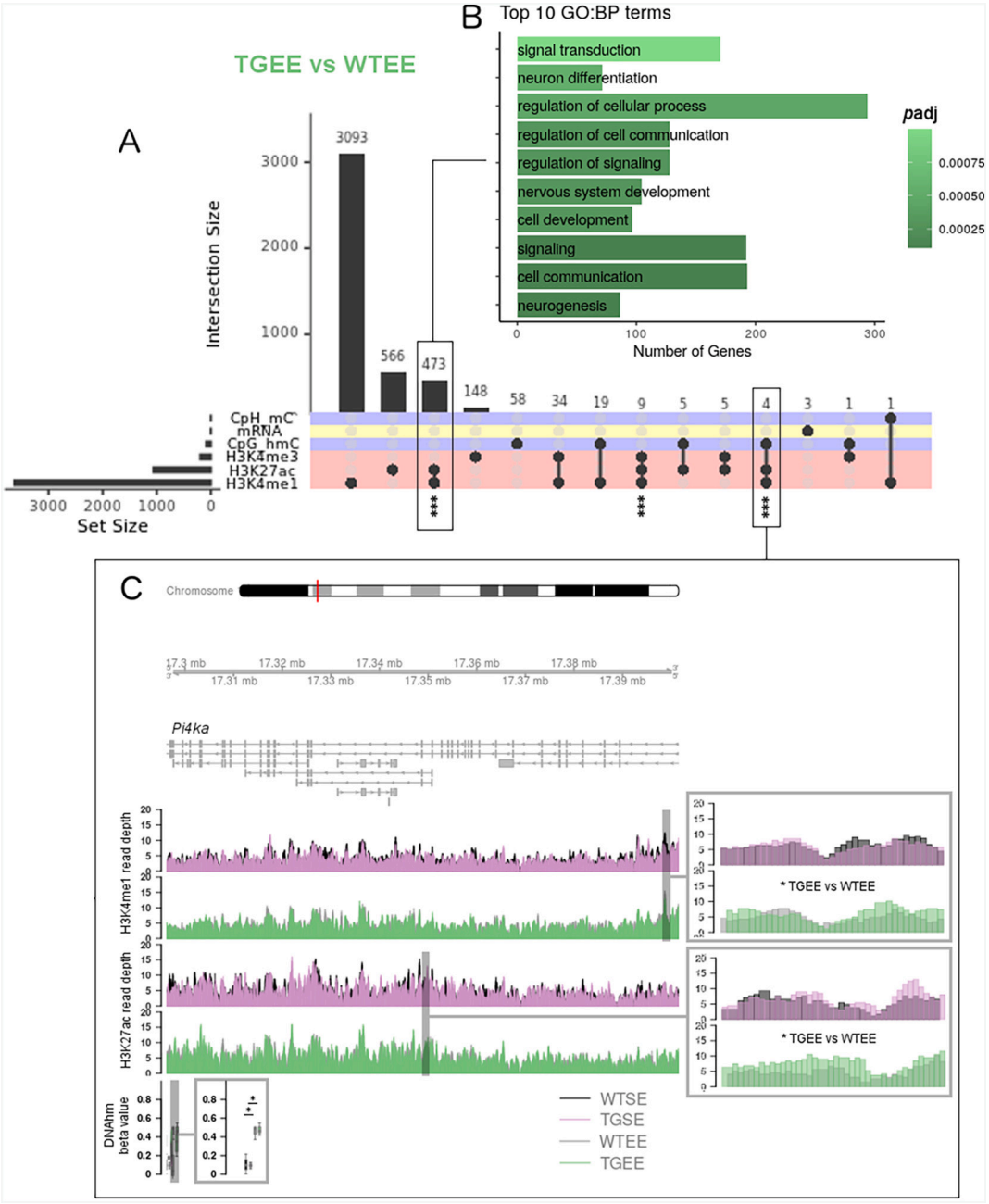

Fig. 8. H3K4 methylation changes in the TG_{EE} vs. WT_{EE} comparison co-occurred with changes to H3K27ac and DNAhm. (A) Overlap in differentially expressed genes, differentially methylated/hydroxymethylated genes, and differentially bound genes for the TG_{EE} vs. WT_{EE} comparison. *** $p_{adj} < 0.001$ (1000 permutations). (B) Top 10 GO Biological Process terms enriched in genes with altered H3K4me1 and H3K27ac in the TG_{EE} vs. WT_{EE} comparison, ranked by significance. (C) *Pi4ka* is shown as an example of a gene with differential H3K4me1, H3K27ac, and DNAhm. Normalized H3K4me1 (top) and H3K27ac (middle) read depths for differentially bound *Pi4ka* peaks, and β values for the differentially hydroxymethylated *Pi4ka* CpG (bottom) are shown. * $p_{adj} < 0.05$.

4.2. Crosstalk between layers of epigenetic regulation

It has been reported that epigenetic marks, including those examined in the present study, are correlated with each other through recruitment of epigenetic modifiers, such as MeCP2, TET1, and histone deacetylases (Kinde et al., 2015; Mellén et al., 2012; Wu and Zhang, 2014; Xu et al., 2011). Although little is known about the impacts of aSyn on H3K4 methylation, CpH methylation, and CpG hydroxymethylation, the overall patterns of increased H3K27ac and decreased CpG hydroxymethylation and H3K4 methylation observed with aSyn overexpression were consistent with the established relations between these epigenetic marks. Despite the fact that we could not determine whether one type of epigenetic alteration may have initiated changes in the others, it is likely that crosstalk between these epigenetic modifications contributed to the overall chromatin remodeling observed with overexpression of aSyn in both environments.

4.3. aSyn–environment interaction

The associations of aSyn overexpression with CpG hydroxymethylation and H3K27ac levels showed similar trends in both SE and EE, while those with CpH and H3K4 methylation differed according to housing environment. Indeed, EE can induce synaptic plasticity, activity-dependent gene transcription, and chromatin remodeling, and

is associated with varying levels of hippocampal neurogenesis in an experience-dependent manner (Wassouf et al., 2018; Zhang et al., 2018). In addition, hippocampal CpH methylation was shown to be associated with environment-dependent neurogenesis and synaptogenesis (Kinde et al., 2015; Lister et al., 2013) and hippocampal H3K4me1 patterns have been implicated in learning and memory formation in rodents and hypothesized to fine-tune environment-dependent gene regulation (Rada-Iglesias, 2018; Rickels et al., 2017; Gandara et al., 2022; Collins et al., 2019). While we were unable to determine the precise mechanisms underlying the gene- and environment-dependent influences on CpH and H3K4 methylation in our model, the correlation between H3K4me1 and mRNA expression levels suggested a contribution of H3K4me1 to a small subset of the preventive effects of EE on gene regulation. Our findings indicating that genotype and genotype–environment interaction were the main contributors to intergroup differences in the epigenomes of mice in this study were consistent with our previous work on the impacts of *SNCA* overexpression and chronic unpredictable mild stress on the striatal transcriptome, and with studies assessing contributions of genotype and environment to DNAm patterns in human populations (Wassouf et al., 2019; Teh et al., 2014; Czamara et al., 2019).

4.4. Cell type-specific impacts of aSyn overexpression

We observed enrichment of differential H3K27ac and H3K4me1 in pyramidal neuron-specific genes in both TG_{SE} vs. WT_{SE} and the TG_{EE} vs. WT_{EE} comparisons. In the same comparisons, we also saw higher levels of differential CpH methylation and CpG hydroxymethylation, both of which are neuron-enriched marks, than differential CpG methylation, which is found in neurons and glia (Kinde et al., 2015). This was consistent with a previous study where we hypothesized that immediate-early gene expression in pyramidal neurons in TG_{EE} mice relative to WT_{SE}, WT_{EE}, and TG_{SE} mice was activated as a compensatory mechanism for decreased synaptic function associated with excess aSyn (Wassouf et al., 2018). However, as few of the epigenetic changes investigated in this study were correlated with the glial cell-specific gene expression disturbances reported previously in TG_{SE} mice, there were likely multiple gene regulatory mechanisms in the various hippocampal cell types comprising our bulk tissue samples (Wassouf et al., 2018). Future studies building upon our results using sorted cell populations and/or assessing additional epigenetic marks are required to gain a more comprehensive picture of the aSyn- and EE-associated chromatin landscape.

4.5. Strengths and limitations

This study revealed wide-ranging impacts of aSyn overexpression and aSyn–environment interactions on the hippocampal epigenome. We also generated new publicly available RRBS data to facilitate further research into mouse models of synucleinopathies (GSE228961). However, several strengths and limitations should be taken into consideration in the interpretation of our results. First, no model can perfectly recapitulate human synucleinopathies, and our study focused primarily on the molecular epigenetic impacts of aSyn expression in the brain. Second, we profiled bulk hippocampal tissue, which is comprised of multiple neuronal and glial cell subtypes that can influence epigenetic patterns. Although experiments using two single-cell RNA-seq data sets to estimate neuronal and glial cell proportions indicated no overall differences in predicted cellular composition between the WT and TG mice profiled in this study, it is still likely that specific cell subpopulations responded to aSyn overexpression and EE, as indicated by our enrichment analysis (Wassouf et al., 2018). Third, although we examined an extensive set of epigenetic marks in this study, this was not exhaustive. We focused on H3K4me1, H3K4me3, and H3K27ac due to their ability to delineate active enhancers and promoters; however, our knowledge of the full range of molecular genetic impacts of aSyn remains incomplete. Fourth, interindividual variation in EE-associated hippocampal neurogenesis between mice may have influenced the extents to which the ChIP-seq data were comparable to the DNA(h)m and RNA-seq data (Kempermann, 2019). However, to reduce these effects as much as possible, we extracted histones from mice housed in the same cages as those from which DNA and RNA were extracted. In addition, our ChIP-seq findings were likely influenced by H3 density. While H3 abundance is not altered by aSyn overexpression in SH-SY5Y cells, it is elevated in the human PD brain; if this was also the case in our mice, elevated H3 may have underpinned increases in H3K27ac or masked additional changes in H3K4 mono- and/or trimethylation (Kontopoulos et al., 2006; Toker et al., 2021; Sugeno et al., 2016). In future studies, this could be measured by H3 ChIP (Cruz et al., 2018). Finally, we used only female mice in this study, and were therefore unable to determine whether there are sex differences in the responses to aSyn and EE. However, increased aggression levels and hierarchical behavior between male mice housed in EE may interfere with its potential benefits, including learning and exploration behaviors (Marashi et al., 2003; Martinez-Cue et al., 2002). Using females facilitated housing of more mice per cage with reduced aggression levels, and thus allowed a more thorough investigation of the impacts of EE on the epigenome.

5. Conclusions

In conclusion, we characterized the impacts of aSyn expression on the hippocampal epigenome in mice housed in either SE or EE. Our results indicated gene feature-dependent DNAhm alterations that were consistent across environments. The large numbers of *SNCA*- and environment-dependent histone modification differences at genes relevant to aSyn biology and synaptic function suggested that *SNCA* overexpression and EE had opposing effects on the hippocampal epigenome, likely affecting multiple cell types. This work complements previous studies assessing DNA and/or histone modifications in the human brain, tissue culture, and rodent models, and provides insights into the effects of increased physical activity and both cognitive and social stimulation on the mammalian brain. Future studies should continue to examine the molecular epigenetic impacts of aSyn expression in different tissues and cell types, to determine whether EE can ameliorate behavioral changes observed in rodent models of PD, and to assess the potential etiological roles of genes impacted by both aSyn and the environment in the development of synucleinopathies.

Funding

The study design and data collection in this study were supported by Canadian Institutes of Health Research [EGM-141897] and the Federal Ministry of Education and Research [01KU1503A]. SS was funded by a Doctoral Research Award from the Canadian Institutes of Health Research (data analysis and manuscript writing). MSK is the Edwin S.H. Leong UBC Chair in Healthy Aging.

Ethical approval

All procedures adhered strictly to international standards for the care and use of laboratory animals and were approved by the local Animal Welfare and Ethics committee of the Country Commission Tübingen, Germany (TVA HG 4/11).

Author contributions

Samantha Schaffner: RRBS library preparation and analysis, multiomics integration, conceptualization, visualization, writing—original draft. Zinah Wassouf: Mouse work, RNA-seq and ChIP-seq library preparation and analysis, conceptualization, writing—review and editing. Thomas Hentrich: ChIP-seq analysis, conceptualization, writing—review and editing. Melanie Nuesch-Germano: ChIP-seq analysis,

writing—review and editing. Michael Kobor: Funding acquisition, supervision, conceptualization, writing—review and editing. Julia Schulze-Hentrich: Funding acquisition, supervision, conceptualization, writing—review and editing.

Code availability statement

All code is publicly available at github.com/samschaf/SNCA_mouse_EE_hippocampus.

CRediT authorship contribution statement

Samantha L. Schaffner: Formal analysis, Visualization, Writing – original draft. **Zinah Wassouf:** Investigation, Formal analysis, Writing – review & editing. **Thomas Hentrich:** Formal analysis, Writing – review & editing. **Melanie Nuesch-Germano:** Methodology, Writing – review & editing. **Michael S. Kobor:** Funding acquisition, Supervision, Conceptualization, Writing – review & editing. **Julia M. Schulze-Hentrich:** Funding acquisition, Supervision, Conceptualization, Writing – review & editing.

Declaration of Competing Interest

The authors declare no competing interests.

Data availability

The raw data supporting the conclusions of this article will be made available by the authors at reasonable request. RNA-seq and RRBS data files have been uploaded to the GEO database and are available under the accession numbers GSE96961 and GSE228961, respectively.

Acknowledgements

The authors wish to acknowledge Canada's Michael Smith Genome Sciences Centre, Vancouver, Canada, for sequencing of mouse RRBS libraries. We thank Alan Kerr, Rui Wang, Maggie Fu, Marcia Jude, and Dr. Mandy Meijer for their valuable comments on the manuscript draft, and Dr. Sarah Merrill for her helpful feedback on conceptualization of the manuscript.

Appendix A. Supplementary data

Supplementary data to this article can be found online at https://doi.org/10.1016/j.nbd.2023.106274.

References

Ascherio, A., Schwarzschild, M.A., 2016. The epidemiology of Parkinson's disease: risk factors and prevention. Lancet Neurol. 15 (12), 1257–1272.
Babraham, Andrews S., 2010. Bioinformatics. In: FastQC: a quality control tool for high throughput sequence data. Available from: https://www.bioinformatics.babraham.ac.uk/projects/fastqc/.
Calabresi, P., Castrioto, A., Filippo, M.D., Picconi, B., 2013. New experimental and clinical links between the hippocampus and the dopaminergic system in Parkinson's disease. Lancet Neurol. 12 (8), 811–821.
Cavalcante, R.G., Sartor, M.A., 2017 Aug 1. annotatr: genomic regions in context. Valencia A, editor. Bioinformatics. 33 (15), 2381–2383.
Chartier-Harlin, M.C., Kachergus, J., Roumier, C., Mouroux, V., Douay, X., Lincoln, S., et al., 2004. Alpha-synuclein locus duplication as a cause of familial Parkinson's disease. Lancet 364 (9440), 1167–1169.
Chen, H., Ritz, B., 2018. The search for environmental causes of Parkinson's disease: moving forward. J. Parkinsons Dis. 8 (s1), S9–17.
Chen, R.H.C., Wislet-Gendebien, S., Samuel, F., Visanji, N.P., Zhang, G., Marsilio, D., et al., 2013. α-Synuclein membrane association is regulated by the Rab3a recycling machinery and presynaptic activity. J. Biol. Chem. 288 (11), 7438–7449.
Chiba-Falek, O., Nussbaum, R.L., 2001. Effect of allelic variation at the NACP-Rep1 repeat upstream of the alpha-synuclein gene (SNCA) on transcription in a cell culture luciferase reporter system. Hum. Mol. Genet. 10 (26), 3101–3109.
Collins, B.E., Greer, C.B., Coleman, B.C., Sweatt, J.D., 2019. Histone H3 lysine K4 methylation and its role in learning and memory. Epigenetics Chromatin 12 (1), 7.
Creyghton, M.P., Cheng, A.W., Welstead, G.G., Kooistra, T., Carey, B.W., Steine, E.J., et al., 2010. Histone H3K27ac separates active from poised enhancers and predicts developmental state. Proc. Natl. Acad. Sci. U. S. A. 107 (50), 21931–21936.
Crotty, G.F., Schwarzschild, M.A., 2020. Chasing protection in Parkinson's disease: does exercise reduce risk and progression? Front. Aging Neurosci. 12, 186.
Cruz, C., Della Rosa, M., Krueger, C., Gao, Q., Horkai, D., King, M., et al., 2018. Tri-methylation of histone H3 lysine 4 facilitates gene expression in ageing cells. Shilatifard A, Tyler JK, editors eLife 7, e34081.
Czamara, D., Eraslan, G., Page, C.M., Lahti, J., Lahti-Pulkkinen, M., Hämäläinen, E., et al., 2019. Integrated analysis of environmental and genetic influences on cord blood DNA methylation in new-borns. Nat. Commun. 10 (1), 2548.
Dobin, A., Davis, C.A., Schlesinger, F., Drenkow, J., Zaleski, C., Jha, S., et al., 2013. STAR: ultrafast universal RNA-seq aligner. Bioinformatics. 29 (1), 15–21.
Du, P., Kibbe, W.A., Lin, S.M., 2008. lumi: A pipeline for processing Illumina microarray. Bioinformatics. 24 (13), 1547–1548.
Espeso-Gil, S., Holik, A.Z., Bonnin, S., Jhanwar, S., Chandrasekaran, S., Pique-Regi, R., et al., 2021. Environmental enrichment induces epigenomic and genome organization changes relevant for cognition. Front. Mol. Neurosci. 5 (14), 664912.
Gandara, L., Tsai, A., Ekelöf, M., Galupa, R., Preger-Ben Noon, E., Alexandrov, T., et al., 2022. Developmental phenomics suggests that H3K4 monomethylation confers multi-level phenotypic robustness. Cell Rep. 41 (11), 111832.
Gu, H., Smith, Z.D., Bock, C., Boyle, P., Gnirke, A., Meissner, A., 2011. Preparation of reduced representation bisulfite sequencing libraries for genome-scale DNA methylation profiling. Nat. Protoc. 6 (4), 468–481.
Hüttenrauch, M., Salinas, G., Wirths, O., 2016. Effects of long-term environmental enrichment on anxiety, memory, hippocampal plasticity and overall brain gene expression in C57BL6 mice. Front. Mol. Neurosci. 9, 62.
Irier, H., Street, R.C., Dave, R., Lin, L., Cai, C., Davis, T.H., et al., 2014. Environmental enrichment modulates 5-hydroxymethylcytosine dynamics in hippocampus. Genomics. 104 (5), 376–382.
Jin, H., Kanthasamy, A., Ghosh, A., Yang, Y., Anantharam, V., Kanthasamy, A.G., 2011. α-Synuclein negatively regulates protein kinase Cδ expression to suppress apoptosis in dopaminergic neurons by reducing p300 histone acetyltransferase activity. J. Neurosci. 31 (6), 2035–2051.
Kempermann, G., 2019. Environmental enrichment, new neurons and the neurobiology of individuality. Nat. Rev. Neurosci. 20 (4), 235–245.
Kempermann, G., Kuhn, H.G., Gage, F.H., 1997. More hippocampal neurons in adult mice living in an enriched environment. Nature. 386 (6624), 493–495.
Kimura, H., 2013. Histone modifications for human epigenome analysis. J. Hum. Genet. 58 (7), 439–445.
Kinde, B., Gabel, H.W., Gilbert, C.S., Griffith, E.C., Greenberg, M.E., 2015. Reading the unique DNA methylation landscape of the brain: non-CpG methylation, hydroxymethylation, and MeCP2. Proc. Natl. Acad. Sci. 112 (22), 6800–6806.
Kolberg, L., Raudvere, U., Kuzmin, I., Vilo, J., Peterson, H., 2020. gprofiler2—an R package for gene list functional enrichment analysis and namespace conversion toolset g: Profiler. F1000Research. 9 (ELIXIR-709).
Kontopoulos, E., Parvin, J.D., Feany, M.B., 2006. Alpha-synuclein acts in the nucleus to inhibit histone acetylation and promote neurotoxicity. Hum. Mol. Genet. 15 (20), 3012–3023.
Langmead, B., Salzberg, S.L., 2012. Fast gapped-read alignment with bowtie 2. Nat. Methods 9 (4), 357–359.
Li, H., Handsaker, B., Wysoker, A., Fennell, T., Ruan, J., Homer, N., et al., 2009. The sequence alignment/map format and SAMtools. Bioinformatics. 25 (16), 2078–2079.
Lister, R., Mukamel, E.A., Nery, J.R., Urich, M., Puddifoot, C.A., Nicholas, D., et al., 2013. Global Epigenomic Reconfi guration during mammalian brain development. Science. 341 (mC), 629–643.
Love, M.I., Huber, W., Anders, S., 2014. Moderated estimation of fold change and dispersion for RNA-seq data with DESeq2. Genome Biol. 15 (12), 550.
Lunnon, K., Hannon, E., Smith, R.G., Dempster, E., Wong, C., Burrage, J., et al., 2016. Variation in 5-hydroxymethylcytosine across human cortex and cerebellum. Genome Biol. 17 (1) https://doi.org/10.1186/s13059-016-0871-x. Available from:
Maraganore, D.M., De Andrade, M., Elbaz, A., Farrer, M.J., Ioannidis, J.P., Krüger, R., et al., 2006. Collaborative analysis of alpha-synuclein gene promoter variability and Parkinson disease. J. Am. Med. Assoc. 296 (6), 661–670.
Marashi, V., Barnekow, A., Ossendorf, E., Sachser, N., 2003. Effects of different forms of environmental enrichment on behavioral, endocrinological, and immunological parameters in male mice. Horm. Behav. 43 (2), 281–292.
Marshall, L.L., Killinger, B.A., Ensink, E., Li, P., Li, K.X., Cui, W., et al., 2020. Epigenomic analysis of Parkinson's disease neurons identifies Tet2 loss as neuroprotective. Nat. Neurosci. 23 (10), 1203–1214.
Martinez-Cue, C., Baamonde, C., Lumbreras, M., Paz, J., Davisson, M.T., Schmidt, C., et al., 2002. Differential effects of environmental enrichment on behavior and learning of male and female Ts65Dn mice, a model for Down syndrome. Behav. Brain Res. 134 (1), 185–200.
Mellén, M., Ayata, P., Dewell, S., Kriaucionis, S., Heintz, N., 2012. MeCP2 binds to 5hmC enriched within active genes and accessible chromatin in the nervous system. Cell. 151 (7), 1417–1430.
Nithianantharajah, J., Hannan, A.J., 2006. Enriched environments, experience-dependent plasticity and disorders of the nervous system. Nat. Rev. Neurosci. 7 (9), 697–709.
Nuber, S., Harmuth, F., Kohl, Z., Adame, A., Trejo, M., Schönig, K., et al., 2013. A progressive dopaminergic phenotype associated with neurotoxic conversion of α-synuclein in BAC-transgenic rats. Brain. 136 (Pt 2), 412–432.
Oliveira, L.M.A., Falomir-Lockhart, L.J., Botelho, M.G., Lin, K.H., Wales, P., Koch, J.C., et al., 2015. Elevated α-synuclein caused by SNCA gene triplication impairs neuronal

differentiation and maturation in Parkinson's patient-derived induced pluripotent stem cells. Cell Death Dis. 6 (11), e1994.
Paiva, I., Pinho, R., Pavlou, M.A., Hennion, M., Wales, P., Schütz, A.L., et al., 2017. Sodium butyrate rescues dopaminergic cells from alpha-synuclein-induced transcriptional deregulation and DNA damage. Hum. Mol. Genet. 26 (12), 2231–2246.
Paiva, I., Jain, G., Lázaro, D.F., Jerčić, K.G., Hentrich, T., Kerimoglu, C., et al., 2018. Alpha-synuclein deregulates the expression of COL4A2 and impairs ER-Golgi function. Neurobiol. Dis. 119, 121–135.
Pidsley, R., Wong, C.C.Y., Volta, M., Lunnon, K., Mill, J., Schalkwyk, L.C., 2013. A data-driven approach to preprocessing Illumina 450 K methylation array data. BMC Genomics 14, 293.
Rada-Iglesias, A., 2018. Is H3K4me1 at enhancers correlative or causative? Nat. Genet. 50 (1), 4–5.
Rickels, R., Herz, H.M., Sze, C.C., Cao, K., Morgan, M.A., Collings, C.K., et al., 2017. Histone H3K4 monomethylation catalyzed by Trr and mammalian COMPASS-like proteins at enhancers is dispensable for development and viability. Nat. Genet. 49 (11), 1647–1653.
Schaffner, S.L., Wassouf, Z., Lazaro, D.F., Xylaki, M., Gladish, N., Lin, D.T.S., et al., 2022. Alpha-synuclein overexpression induces epigenomic dysregulation of glutamate signaling and locomotor pathways. Hum. Mol. Genet. 00 (May), 1–21.
Shehadeh, L.A., Yu, K., Wang, L., Guevara, A., Singer, C., Vance, J., et al., 2010. SRRM2, a potential blood biomarker revealing high alternative splicing in Parkinson's disease. PLoS One 5 (2), e9104.
Stark, R., Brown, G., 2011. Bioconductor. In: DiffBind: Differential Binding Analysis of ChIP-Seq Peak Data.
Sugeno, N., Jäckel, S., Voigt, A., Wassouf, Z., Schulze-Hentrich, J., Kahle, P.J., 2016. α-Synuclein enhances histone H3 lysine-9 dimethylation and H3K9me2-dependent transcriptional responses. Sci. Rep. 3 (6), 36328.
Suzuki, R., Shimodaira, H., 2006. Pvclust: an R package for assessing the uncertainty in hierarchical clustering. Bioinformatics. 22 (12), 1540–1542.
Teh, A.L., Pan, H., Chen, L., Ong, M.L., Dogra, S., Wong, J., et al., 2014. The effect of genotype and in utero environment on interindividual variation in neonate DNA methylomes. Genome Res. 24 (7), 1064–1074.
Toker, L., Tran, G.T., Sundaresan, J., Tysnes, O.B., Alves, G., Haugarvoll, K., et al., 2021. Genome-wide histone acetylation analysis reveals altered transcriptional regulation in the Parkinson's disease brain. Mol. Neurodegener. 16 (1), 31.
van Iterson, M., van Zwet, E.W., Heijmans, B.T., the BIOS Consortium, 2017. Controlling bias and inflation in epigenome- and transcriptome-wide association studies using the empirical null distribution. Genome Biol. 18 (1), 19.
Vemuri, P., Fields, J., Peter, J., Klöppel, S., 2016. Cognitive interventions in Alzheimer's and Parkinson's diseases: emerging mechanisms and role of imaging. Curr. Opin. Neurol. 29 (4), 405.
Villar-Piqué, A., Lopes da Fonseca, T., Outeiro, T.F., 2016. Structure, function and toxicity of alpha-synuclein: the Bermuda triangle in synucleinopathies. J. Neurochem. 139 (Suppl. 1), 240–255.
Warnes, G.R., Bolker, B., Bonebakker, L., Gentleman, R., Huber, W., Liaw, A., et al., 2022. gplots: Various R Programming Tools for Plotting Data [Internet] [cited 2023 Jun 22]. Available from: https://cran.r-project.org/web/packages/gplots/index.html.
Wassouf, Z., Schulze-Hentrich, J.M., 2019. Alpha-synuclein at the nexus of genes and environment: the impact of environmental enrichment and stress on brain health and disease. J. Neurochem. 150 (5), 591–604.
Wassouf, Z., Hentrich, T., Samer, S., Rotermund, C., Kahle, P.J., Ehrlich, I., et al., 2018. Environmental enrichment prevents transcriptional disturbances induced by alpha-synuclein overexpression. Front. Cell. Neurosci. 12, 112.
Wassouf, Z., Hentrich, T., Casadei, N., Jaumann, M., Knipper, M., Riess, O., et al., 2019. Distinct Stress Response and Altered Striatal Transcriptome in Alpha-Synuclein Overexpressing Mice, 12, pp. 1–14. January.
Wu, H., Zhang, Y., 2014. Reversing DNA methylation: mechanisms, genomics, and biological functions. Cell. 156 (0), 45–68.
Xi, Y., Li, W., 2009. BSMAP: whole genome bisulfite sequence MAPping program. BMC Bioinforma. 10, 1–9.
Xu, Y., Wu, F., Tan, L., Kong, L., Xiong, L., Deng, J., et al., 2011. Genome-wide regulation of 5hmC, 5mC and gene expression by Tet1 hydroxylase in mouse embryonic stem cells. Mol. Cell 42 (4), 451–464.
Yamakado, H., Moriwaki, Y., Yamasaki, N., Miyakawa, T., Kurisu, J., Uemura, K., et al., 2012. α-Synuclein BAC transgenic mice as a model for Parkinson's disease manifested decreased anxiety-like behavior and hyperlocomotion. Neurosci. Res. 73 (2), 173–177.
Yu, G., Wang, L.G., He, Q.Y., 2015. ChIPseeker: an R/Bioconductor package for ChIP peak annotation, comparison and visualization. Bioinformatics. 31 (14), 2382–2383.
Zeisel, A., Muñoz-Manchado, A.B., Codeluppi, S., Lönnerberg, P., La Manno, G., Juréus, A., et al., 2015. Cell types in the mouse cortex and hippocampus revealed by single-cell RNA-seq. Science. 347 (6226), 1138–1142.
Zhang, T.Y., Keown, C.L., Wen, X., Li, J., Vousden, D.A., Anacker, C., et al., 2018. Environmental enrichment increases transcriptional and epigenetic differentiation between mouse dorsal and ventral dentate gyrus. Nat. Commun. 9 (1), 298.
Zocher, S., Overall, R.W., Lesche, M., Dahl, A., Kempermann, G., 2021. Environmental enrichment preserves a young DNA methylation landscape in the aged mouse hippocampus. Nat. Commun. 12 (1), 3892.